THESIS FOR THE DEGREE OF LICENTIATE OF ENGINEERING

Battery thermal management for electric vehicles operating in cold climates

ANANDH RAMESH BABU

Department of Mechanics and Maritime Sciences

CHALMERS UNIVERSITY OF TECHNOLOGY

Göteborg, Sweden 2022

Battery thermal management for electric vehicles operating in cold climates
ANANDH RAMESH BABU

Thesis for the degree of Licentiate of Engineering 2022:03
Department of Mechanics and Maritime Sciences
Chalmers University of Technology
SE-412 96 Göteborg
Sweden
Telephone: +46 (0)31-772 1000

Chalmers Digitaltryck
Göteborg, Sweden 2022

Battery thermal management for electric vehicles operating in cold climates
ANANDH RAMESH BABU
Department of Mechanics and Maritime Sciences
Chalmers University of Technology

Abstract

Electromobility has gained significance over recent years in an attempt to reduce greenhouse gas emissions which contribute to climate change. The requirements on the performance and efficiency of electric vehicles are high to make them an attractive alternative to the conventional fossil-fuel driven vehicles. Lithium-ion batteries are the primary energy source for electric vehicles as they have high power and energy density, excellent storage capabilities and long cycling life when operated under conducive conditions, i.e a temperature range of 15°C to 35°C. However, their performance and cycling life are drastically affected when the operating temperature is outside this range. Therefore, battery packs must be heated to optimal temperatures under cold climates. This energy is often provided by the packs themselves, which results in reduced driving range.

This work investigates thermal encapsulation of battery packs as a means of passive battery thermal management to improve the battery performance and decrease heating demand during the initial phase of driving in cold climates. In order to predict the effects of battery pack encapsulation, a robust battery model that captures the dynamic behaviour of large battery packs is necessary in addition to other simplified vehicle and powertrain subsystems. The presented work proposes an integrated simulation methodology that enables numerical simulation of the relevant phenomenon at battery module, powertrain and vehicle levels.

The battery modeling strategy uses a one-dimensional module discretized electrical-thermal approach. An electrical circuit model with 2RC Thevenin branches was used to capture the electrical performance and the Bernardi's heat generation equation was used to estimate the heat generated from each module. The developed strategy was found to be in good agreement with measured test data. Vehicle simulations were performed under parking-driving scenarios to investigate the effectiveness of battery pack encapsulation at different ambient temperatures. It was found that the percentage of energy saved with battery pack encapsulation increased with decreasing ambient temperatures. The thermal resistance of the encapsulation material played a significant role in reducing heat loss to the environment. The simulations indicated that there is a potential of approximately 15% energy savings as a result of increased initial battery temperatures.

Keywords: electric vehicle, lithium-ion battery, battery modeling, low-temperature performance, battery pack encapsulation

Acknowledgements

I would like to express my utmost gratitude to all those, who made this work possible and helped me during my studies. I would like to acknowledge the Swedish Energy Agency, VGTT and VCC for their funding, and Prof. Lennart Löfdahl and Alexander Broniewicz without whom this project would not have been possible.

First of all, I would like to thank my examiner Prof. Simone Sebben for all the constant guidance and support through the different stages of my education. I would also like to thank Ph.D Jelena Andric for her patience, cooperation and continuous feedback especially with regards to the writing process. I would like to extend my gratitude to all my industrial supervisors who have shown great interest in my work so far. Ph.D Blago Minovski, VGTT for all his invaluable knowledge and expertise on thermal management in electric vehicles and ensuring me with the necessary resources to carryout the work. I would also like to acknowledge Prof. Sassan Etemad, VGTT and Tore Bark, VCC for the support and cooperation in the later stages of the project.

I would like to thank Ph.D Masih Khoshab, VGTT and Ph.D Majid Astaneh for their invaluable inputs and for helping me learn about battery modeling.

Furthermore, I want to show my deepest appreciation to all my former and present colleagues, and friends at VEAS for creating an excellent work environment incorporating both academic and entertaining discussions which have made the past two years delightful despite these challenging times. I would like to thank Sonja for her constant support and bringing everyone together for all the fun activities.

To all my friends and especially my family, a big thank you for supporting, inspiring and putting up with me all these years.

Anandh Ramesh Babu
Göteborg, February 2022

Nomenclature

Abbreviations

1D	One-dimensional
3D	Three-dimensional
BEV	Battery electric vehicle
BTMS	Battery thermal management system
CFD	Computational fluid dynamics
ECM	Electrical circuit model
EPA	Environmental Protection Agency
EV	Electric vehicle
GHG	Green house gas
GT	Gamma technologies
HWFET	Highway fuel economy test
IC	Internal combustion
LIB	Lithium-ion battery
NMC	Nickel-Manganese-Cobalt
PCM	Phase change material
PNGV	Partnership for new generation of vehicles
PTC	Positive thermal coefficient
RC	Resistance-capacitance
RMS	Root mean square
TIM	Thermal interface material
VCC	Volvo car corporation
VGTT	Volvo group truck technology

Symbols

α	Road gradient	$[rad]$
Δt (or dt)	Time step	$[s]$
η_b	Efficiency of the battery	$[-]$
μ_r	Tyre rolling resistance	$[-]$
ω	Motor angular velocity	$\left[\frac{rad}{s}\right]$
τ	Motor torque	$[N.m]$

a_v	Vehicle acceleration	$\left[\frac{m}{s^2}\right]$
A_{f_v}	Vehicle frontal area	$[m^2]$
C	Capacity	$[A.h]$
C_d	Drag coefficient	$[-]$
C_i	Polarization capacitance in the ECM	$[F]$
c_p	Specific heat capacity	$\left[\frac{J}{kg.K}\right]$
g	Acceleration due to gravity	$\left[\frac{m}{s^{-2}}\right]$
I	Current	$[A]$
k	Thermal conductivity	$\left[\frac{W}{m.K}\right]$
M_v	Vehicle mass	$[kg]$
P_v	Vehicle traction power	$[W]$
Q^*	Non-dimensionalized coolant volume flow rate	$[-]$
Q_{ref}	Reference coolant volume flow rate	$\left[\frac{l}{min}\right]$
R_{int}	Cell internal resistance	$[\Omega]$
SoC	State of charge	$[\%]$
SoC_0	Initial state of charge	$[\%]$
t^*	Non-dimensionalized time	$[-]$
T^*	Non-dimensionalized temperature	$[-]$
T_{ref}	Reference temperature	$[K]$
U_{oc}	Open-circuit voltage	$[V]$
V	Terminal voltage	$[V]$
v_v	Vehicle velocity	$\left[\frac{m}{s}\right]$
$\dot{Q}_{net}$	Net rate of heat accumulation in a thermal mass	$[W]$
$\frac{dU_{oc}}{dT}$	Battery entropic coefficient	$\left[\frac{V}{K}\right]$
$\frac{D}{Dt}$	Total derivative	$[s^{-1}]$
μ	Dynamic viscosity	$[Pa.s]$
ρ	Material density	$\left[\frac{kg}{m^{-3}}\right]$
$\vec{U}$	Fluid velocity	$\left[\frac{m}{s}\right]$
A_c	Surface contact area	$[m^2]$
C_f	Friction factor	$[-]$
C_{th}	Thermal capacitance	$\left[\frac{J}{m^3.K}\right]$
h	Heat transfer coefficient	$\left[\frac{W}{m^2K}\right]$
j_{th}	j-factor	$[-]$

m	Mass of a lumped unit	$[kg]$
N_{mod}	Number of cells in a battery module	$[-]$
Nu_D	Nusselt number based on channel diameter	$[-]$
P	Pressure	$[Pa]$
Pr	Prandtl number	$[-]$
Q	Heat transferred	$[J]$
R_i	Polarization resistance in the ECM	$[\Omega]$
R_{th}	Thermal resistance	$[\frac{K}{W}]$
Re_D	Reynold's number based on channel diameter	$[-]$
T	Temperature	$[K]$
t	Thickness of battery pack encapsulation	$[m]$
T_f	Fluid temperature	$[K]$
T_w	Wall temperature	$[K]$
t_{TIM}	Thickness of the thermal interface material	$[m]$
U_i	Voltage drop across i^{th} RC branch in the ECM	$[V]$
C-rate	Charge/discharge current relative to the nominal battery capacity	$[h^{-1}]$

Thesis

This thesis consists of an extended summary of the following appended papers:

Paper A Ramesh Babu, A., Andric, J., Minovski, B., and Sebben, S. "System-Level Modeling and Thermal Simulations of Large Battery Packs for Electric Trucks". *Energies* **14**.16 (2021), 4796

Paper B Ramesh Babu, A., Andric, J., Minovski, B., and Sebben, S. "Thermal encapsulation of large battery packs for electric vehicles operating in cold climate". *Submitted to Applied Thermal Engineering* (2022)

Division of work

A The battery pack was modelled by Ramesh Babu in collaboration with VGTT. The simulations and analysis for Paper A were done by Ramesh Babu. The battery modeling parameters and the experimental data used to validate the model were obtained from VGTT. The first manuscript was written by Ramesh Babu then discussed, reviewed and revised by all authors.

B The modeling, simulation and analysis for Paper B were performed by Ramesh Babu. The electrical circuit battery model was created by VGTT. The first manuscript was written by Ramesh Babu then discussed, reviewed and revised by all authors.

Contents

Part I

Extended summary

1

Introduction

1.1 Background

With global demand for energy resources increasing due to economic growth, the risk of energy crisis and environmental pollution is on the rise as the majority of energy for the transport sector is still derived from fossil fuels [3, 4]. Additionally, the dependence on road vehicles is at an all-time high as the world heads towards a lifestyle that strives for better connectivity and transportation of goods. As a result, the greenhouse gas (GHG) emissions from road vehicles constituted about 72% of the overall GHG emissions from the transport sector in 2019 [5]. The emission cap for road vehicles has decreased with each new regulation and it is expected to reduce further in the coming years to combat the harmful effects of GHG emissions and climate change [6].

Electric vehicles (EVs) have been gaining significance over the past decade and they are viewed as a promising transportation means instead of the conventional vehicles which are driven by fossil fuels. In a study by Andersen et al. [7], it was pointed out that EVs could potentially reduce the GHG emissions from the transport sector by 20% and further up to 40% if the electricity used is generated from renewable sources. Battery electric vehicles (BEVs) also have low operating costs, high performance and efficiency which appeal to the customers. More importantly, opportunities in the form of government subsidies and funding have contributed to the shift in focus to develop and utilize electrified vehicles. A growth of 15-30% in the market share of electric vehicles has been predicted from 2020 to 2030 as shown in Fig. 1.1 [8].

The fundamental challenge for clean energy vehicles to be commercialized is energy storage. Lithium-ion batteries (LIBs) have become the dominant battery technology for the automotive industry as they have a high energy density, high power, excellent storage capabilities and long cycling life. While these are compelling features, LIBs are limited due to safety concerns and rampant costs due to ageing, that are associated with thermal effects. Batteries are electrochemical systems and their performance is highly influenced by their operating temperature. The ideal operating temperature for LIBs is between 15°C to 35°C, and operating outside this range results in poor performance, degradation, and in some extreme cases thermal runaway. Battery packs operating in cold

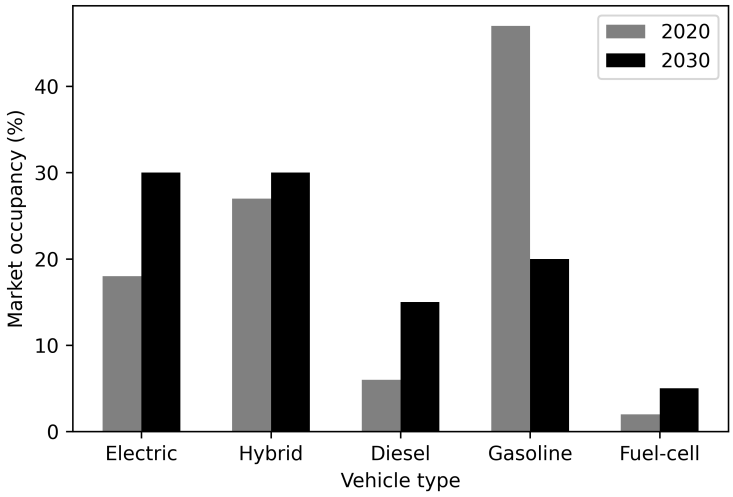

Figure 1.1: *Global market occupancy of vehicles [8].*

climates experience increased impedance, poor discharge/charge capacity and often spend an enormous amount of energy on heating themselves. Additionally the cabin of BEVs must be climatized at low ambient temperatures using the energy from the battery packs, thus shortening the driving range. This is a major deterrent to their market penetration. Hence, improving the thermal efficiency and heat management in BEVs are essential to realize the full potential of their range and performance even at low ambient temperatures.

This project has been derived from the concept of engine encapsulation in IC-engine powered vehicles to improve their cold start performance. By encapsulating the engine, the magnitude of heat transfer between the various parts of the engine and ambient air is reduced. This increases the probability of starting at a higher initial temperature which reduces the friction losses that occurs during cold-start [9]. Analogously, the main objective of this project is to study the effect of encapsulation of the heat-generating components in BEVs, such as battery packs, on their performance and efficiency by aiding them to start at higher initial temperatures.

1.1.1 Working principle of LIBs

A lithium-ion cell is typically comprised of a positive electrode (cathode), a negative electrode (anode), an electrolyte, a separator, current collectors and a case. The type of electrodes used in the cells determines the capacity and energy density of the battery. The positive electrode is made of a lithium compound such as $LiCoO_2$ (LCO), $LiFePO_4$ (LFP), $LiNi_{1-x-y}Mn_xCo_yO_2$ (NMC) and so on while the negative electrode is typically made of carbonaceous compounds such as coke and graphite [10]. The electrolyte is a solution of lithium salt in a non-aqueous solvent such as ethylene carbonate or diethylene carbonate. The current collectors for the positive and negative electrodes are aluminium

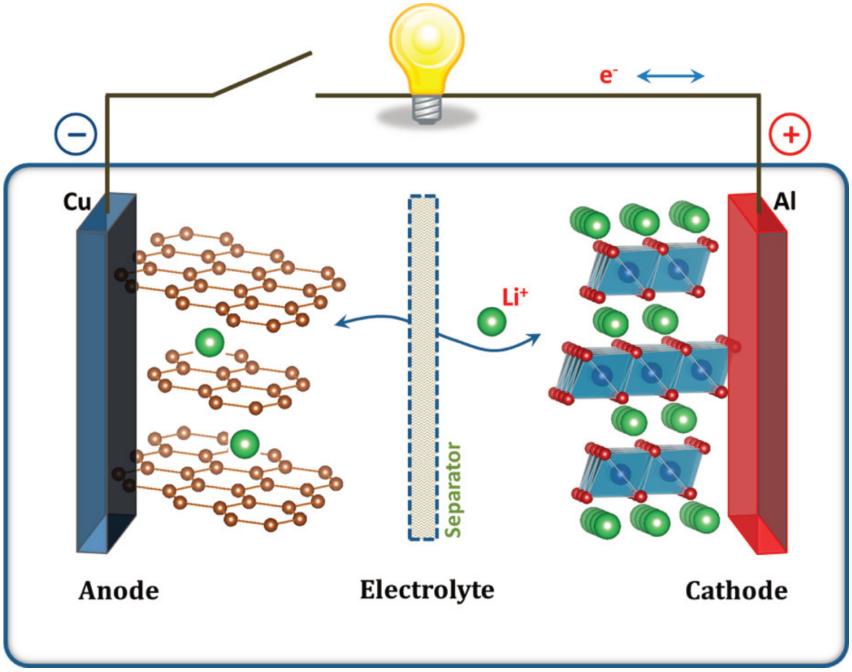

Figure 1.2: *Schematic illustration of a lithium ion cell [12].*

and copper respectively [11]. Figure 1.2 illustrates a schematic of a typical Li-ion cell. The charge/discharge process is characterized by the transport of lithium ions and electrons. During charging, lithium ions are transferred from the positive electrode to the negative electrode through the electrolyte and the separator. Simultaneously, an equal number of electrons released on the positive electrodes are transferred to the negative electrode through the current collector and the external circuit, which forms the charge current. During discharge, an equal amount of lithium ions and electrons are transferred from the negative electrode to the positive electrode through the internal and external circuits, respectively.

1.1.2 Battery modeling approaches

Battery modeling is complex and requires knowledge from different disciplines to understand the governing physics behind it. There exist several categories of battery models that can predict battery behavior with different levels of accuracy. The two most common categories are the electrochemical and equivalent circuit models. The electrochemical model is typically employed to describe the electrochemical reactions, transport phenomena and heat dissipation at the cell level [13–15]. The model was established to formulate the one-dimensional transport of lithium ions between the electrodes through the separator. While being the most detailed and accurate, it is time-consuming and hence not suitable for the analysis of battery thermal management systems (BTMS) in large battery packs. Equivalent circuit models, which use empirical equations modeled using experimental data, perform reasonably well for highly dynamic simulations and run faster than electrochemical models [16]. The equivalent circuit model utilizes resistors, capacitors and voltage sources

to form a circuit network that captures the behaviour of the cells. Typical equivalent circuit models are Rint models (internal resistance model), Resistance-Capacitance (RC) models, Thevenin models and Partnership for New Generation of Vehicles (PNGV) models. The Thevenin model has been widely accepted and it was developed based on the simple Rint model, but with the inclusion of parallel resistor-capacitor branches to account for voltage polarization [17, 18]. Various models have been proposed and verified, among which the Thevenin model was deemed to be adequately accurate for coupled electrical-thermal studies involving battery thermal management systems [10].

Several modeling and simulation studies have been conducted to predict and analyze the thermal behavior of Li-ion cells. Battery heat is generated due to activation, concentration and ohmic losses [19]. The battery thermal model for heat/energy balance accounts for heat accumulation, convection, conduction through the electrolyte/electrodes and heat generation. Whereas, the lumped mass approach is based on heat balance between heat generation, dissipation and accumulation. In this approach, the battery is assumed to have uniform temperature distribution in all directions. The local heat generation model which can be linked to the electrochemistry of cells has been found to be the most accurate approach for heat generation modeling which includes irreversible heat, entropic change, ohmic heat from the solid phase and the electrolyte phase. Bernardi et al [20] formulated a heat generation equation based on the thermodynamic energy balance of a single cell which has been readily accepted. This equation uses the irreversible Joule heating (losses due to internal resistance) and the entropic heat coefficient (variation of open-circuit voltage with temperature) to determine heat generation from cells at a given operating condition.

Many studies have employed coupled electrical/electrochemical-thermal models for studying the behavior of battery modules and packs in both three-dimensional (3D) and one-dimensional (1D) approaches. Wang et al. [21] presented an overview of the vast theoretical research on 3D modeling of batteries. Basu et al. proposed a novel temperature correlation based on a coupled electrochemical 3D CFD model, which can predict the temperature of all the cells in a battery pack based on the measurement of one cell temperature [22]. Saqli et al. [23] presented the modeling methodology of a 1D electrochemical model coupled with a 3D CFD approach to study the thermal behavior of cylindrical cells and later built a thermal first-order equivalent circuit model. For thermal simulations of large-scale EV battery packs, heat is assumed to be generated within the solid domain representing the cells and then transferred to the surrounding medium under the assumption that the internal cell conditions and temperature are homogeneous (lumped approach). Makinejad et al. [24] studied the temperature distribution of cells under different discharge rates for Li-ion pouch cells and found that for current rates under 5 C, the temperature differences in the cells remain under 1°C. Modeling the cells using the lumped approach yielded good agreement with the measured surface temperatures in their study. Alhanouti et al. [25] proposed a new model to accurately estimate the reversible part of heat generated in Bernardi's model [20]. A lumped thermal model was implemented to simulate the development of temperature in a cell and later extended

it to a pack. Gao et al. [26] used an equivalent circuit model in combination with a convective thermal model to estimate the electrical parameters and the temperature of the cells in a 12-cell battery pack. Gottapu et al. [27] proposed a simplified electrochemical model and lumped thermal model to analyze the thermal distribution at the pack level. Shabani et al. [28] presented an overview of the different theoretical, numerical and analytical approaches to thermal modeling in batteries. Recently, Astaneh et al. [29] presented a novel module-to-module discretized modeling framework that employed a coupled electrochemical-thermal battery model. The proposed framework made it possible to capture the temperature non-uniformities with the purpose of performing studies that couple the cell properties to the pack's performance.

1.1.3 Low-temperature effects on battery and vehicle performance

Numerous studies have attempted to investigate the poor performance of LIBs at low temperatures, however the exact mechanisms leading to these effects are still not well understood. Nonetheless, it is clear that their energy and power capabilities are severely decreased at low temperatures. Nagasubramanian [30] studied the performance of the commercial 18650 Li-ion cell and he reported an energy density of 5% and power density of 1.25% at -40°C as compared to 25°C. Zhang et al. [31] linked the poor performance of battery cells at low temperatures to the poor charge transfer at the electrode/electrolyte interface. Their study also suggested that low charge transfer led to significant lithium plating on the negative electrode during charging, which caused irreversible capacity loss. Fan et al. [32] studied charging characteristics at low temperatures and found that significant lithium plating, which occurred when charging at low temperatures, led to an irreversible decrease in battery capacity. They also recommended avoiding charging at high C-rates at these temperatures to limit capacity fade. Bandhauer et al. [19] reviewed the temperature effects on capacity loss and concluded that the charge transfer degraded rapidly with decrease in temperature and that the slow charge transfer at the electrode/electrolyte interface caused the poor low-temperature performance of the cells. Petzl et al. [33] focused on the non-destructive characterization of the fading behaviour of the battery cells during long-term cycling. They elucidated the lithium plating effects on the graphite anode as the most severe factor leading to capacity fade in LIBs at low temperature, where the loss of cyclable active lithium material led to capacity decay. To summarize, the poor performance of LIBs in cold climates can be attributed to four main factors [11]:

1. Low conductivity of the electrolyte and solid electrolyte interface on the electrode surface [34, 35].

2. Declined solid-state Li diffusivity [31, 36].

3. High polarisation of the graphite anode [37, 38].

4. Sluggish kinetics caused by high charge-transfer resistance on the electrode interfaces [31, 36].

In EVs, these effects reduce the driving range and lifetime of the battery pack. Shidore and Bohn [39] quantified the impact of low ambient temperatures at 0°C and -7 °C on battery performance in hybrid electric vehicles. They found a 34% reduction in battery power and an 8-12% increase in internal resistance at these temperatures as compared to an ambient temperature of 20°C. At low temperatures, a large portion of the energy is spent on heating the battery packs and the cabin, thus shortening the driving range by more than 30-40%. [40, 41]. Yuksel et al. showed that the average range in a Nissan Leaf fell from 70 to 45 miles in the cold upper Midwest as compared to the warmer Pacific coast in the US [42]. The drop in range was mainly due to cabin conditioning and poor battery performance. Taggart [43] analyzed over 10,000 Tesla Model S and observed energy consumption increased by over 45% at -10°C. Short trips particularly exhibited higher consumption due to the transient battery and cabin heating energy demand. Testing by Transport Canada of BEV performance under cold conditions at -7°C and -18°C/-20°C using dynamometer drive-cycle operations showed a 50% reduction in range at -18°C/-20°C with heating as compared to a 20°C operation with no heating employed [44]. At -7°C, the use of cabin heating reduced the driving range by about 25% versus no cabin heating at -7°C. Recently, Steinstraeter [45] et al. studied the impact of cabin heating demand and limited battery capacity to recuperate energy at low temperatures in the Tesla Model 3 and in the BMW i3. The results showed a 32% decrease in range due to heating demand and a 22% decrease due to limited recuperation, giving a combined maximum decrease of about 50% under cold conditions.

1.1.4 Battery thermal management strategies

Several battery thermal management strategies have been proposed to climatize the battery packs at their optimal temperature range which include air, liquid, refrigerant, phase change material and heat pipes. While liquid cooling systems pose challenges such as high cost, weight and spatial requirements, they provided better performance allowing high heat transfer rate, effective temperature uniformity of cells in a pack and heating capabilities in cold climates. The liquid cooling strategy can be divided into two types, namely direct and indirect methods. The direct method cools the cells by directly submerging them in a liquid without separators while the indirect method separates the liquid from the cells using a separator in the form of a cooling plate and channels. Chen et al. [46] compared the thermal performance of forced air convection, fin cooling, direct and indirect cooling strategies, and noted that the former method required the highest parasitic cost among all. Additionally, it was found that the indirect strategy was found to be a better choice than direct liquid cooling for vehicle applications. Numerous studies have looked into identifying the optimal geometry of the cooling channels in the indirect liquid-cooled approach. Jarrett and Kim [47] discussed the geometry optimization of a serpentine-channel cold plate design by adjusting the channel width and location for optimal temperature uniformity, mean temperature and pressure drop. They later

discussed the influence of boundary conditions on the optimized designs [48]. Zhu et. al [49] optimized the inlet temperature and mass flow rate of the coolant for the maximum temperature and temperature difference under cooling, and least time and temperature difference under heating conditions in real EV applications. Others have investigated the effect of channel properties on cell temperature, pressure drop of the coolant and energy consumption [50–52].

In order to mitigate the low-temperature effects of LIBs, preconditioning them to optimum temperature before they are cycled has been suggested. The main criteria for the selection of the appropriate heating system are (a) heating time; (b) the power consumption; (c) the overall cost of the system; and (d) the complexity of design [10]. Ji and Wang [53] categorized the heating methods into two types based on the origin of energy: internal and external heating. The internal heating methods included self-heating, convective heating and mutual pulse heating which use energy from the battery pack to heat the cells. As previously stated, the battery internal resistance is greatly increased at lower temperatures, which results in high heat generation. Self-heating methods take advantage of this to heat the cells. Convective heating uses energy from the pack to power an electric heater, which heats the pack itself. Coolant heaters in the form of positive temperature coefficient (PTC) heaters have been used in many studies to heat-up the battery due to quick heat-up time and convenience, and are commonly adopted in EV applications [40, 41]. The mutual pulse heating divided the battery pack into two groups with same capacity where one group discharges to charge the other group. The discharge-charge cycles are alternated to heat up the battery. This method was found to be highly efficient and produced a uniform temperature distribution [54, 55]. Zhang et al. [56] proposed a PTC self-heating method where the LIB was heated with PTC materials placed between cells using battery power. They showed that such a strategy achieved uniform temperature distribution during heat-up. Heating with external power sources eliminated the need for energy consumption from the battery pack, thus extending the driving range. Hand and Stuart [57, 58] proposed a method to heat the batteries with alternating load current. Different amplitudes and frequencies of the alternating current were tested and they found that a frequency of 10-20 kHz and high amplitudes decreased the heat-up time significantly. Additionally, Zhu et al. [59] found that the waveforms of the alternating current also had significant impact on the heating efficiency of LIBs.

While heating with external power sources is best suited for BEVs, it is impractical to rely solely on them to climatize the batteries. Hu et al. [60] pointed out that effective insulation can reduce heat loss to the environment, thus reducing the energy expenses during the warm-up phase. Ling et al. [61] investigated the effect of phase change materials (PCM) with high thermal capacitance to store heat. It was noted that the usage of PCM decreased the rate at which the cells cool down, but negatively affected the heat-up performance of already cold battery cells. Ouyang et al. [62] carried out a series of experiments to probe the influence of thermal insulation around battery cells for the temperature range 0-20°C and concluded that thermally insulated cells showed improved discharge performance and a slower decay rate. Recently, Wu et al. [63] examined the effect of thermal insulation

using nano-porous aerogel with different thicknesses in battery cells. The low thermal diffusivity of the aerogel aided in retaining heat in the cells at low temperatures resulting in better energy utilization.

1.2 Research objectives

The objectives of this thesis are to increase the knowledge on battery modeling, vehicle performance in cold climate, and to comprehend the scope of battery pack encapsulation as a design choice with focus on energy consumption during operation in electric vehicles and extend driving range. In this regard, the goal is divided into two specific research questions:

- What is a suitable modeling strategy to capture the dynamic thermal effects of the battery pack while accounting for other subsystems at the vehicle level?
- How does thermal encapsulation of battery packs affect the energy consumption of EVs at low temperatures?

1.3 Limitations

The modeling strategy used is one-dimensional to facilitate the simulation of different subsystems such as the vehicle powertrain, battery and cooling system in the same platform. While the model has been calibrated to experimental data, 3D effects of heat and fluid flow within/outside the battery pack cannot be captured. The vehicle and system controllers used are quite simplified and low-fidelity models. Additionally, the battery pack encapsulation has been applied to all the sides of the battery casing, something that would be hard to achieve because of support structures, electrical connections, coolant hoses and other packaging issues.

1.4 Outline

The thesis is divided into two sections, where Part-I summaries the work and Part-II includes two articles produced so far. In part-I, Chapter-1 provided context and background to the work, and stated the objectives and limitations of the thesis. Chapter-2 covers the theory and modeling strategy for the various subsystems in the vehicle. Chapter-3 focuses the effects of encapsulation of the battery pack on the performance of the vehicle. Chapter-4 gives some concluding remarks and an outlook into the future work.

2

Modeling framework

2.1 Battery pack modeling

The geometries of the battery pack and the module assembly are shown in Fig. 2.1. The considered battery system is used to truck application and has a 180s2p configuration (where s stands for the number of cells in series and p stands for the number of parallel branches) with an indirect liquid cooling strategy. The pack consists of two trays, placed one on top of the other. Each tray includes battery modules, an aluminium cooling plate and a thermal interface material between the module casings and the cooling plate as shown in Figure 2.1b. Each module has several prismatic NMC-111 type Li-ion cells. The cooling plates have two common railings, one connected to the inlet and the other connected to the outlet. The railings are connected to rows of U-shaped channels. Every row consists of three micro-channels that are used to cool the modules. The whole setup is enclosed in a stainless steel casing (not shown in the figure).

Each coolant microchannel was discretized into seven tubes that the coolant, a 40-60 mixture of glycol-water, flows through. The incompressible conservation equations, namely continuity, momentum and energy as seen in eqn. 2.1-2.3, respectively, were solved numerically to compute the fluid and heat flow in the model using the commercial simulation platform GT-SUITE [64]:

$$\text{Continuity equation:} \quad \nabla \cdot \vec{U} = 0 \tag{2.1}$$

$$\text{Momentum equation:} \quad \rho \frac{D\vec{U}}{Dt} = \nabla P + \nabla \cdot (\mu \nabla \vec{U}) \tag{2.2}$$

$$\text{Energy equation:} \quad \rho c_p \frac{DT}{Dt} = \nabla \cdot (k \nabla T) \tag{2.3}$$

where $\vec{U}$ is the velocity of the fluid, ρ is the density, $\frac{D}{Dt}$ is the total derivative of the quantity ($\frac{D}{Dt}$=$\frac{\partial}{\partial t} + (\vec{U} \cdot \nabla)$), ∇P is the pressure gradient, μ is the dynamic viscosity, c_p is the specific heat capacity, T is the temperature and k is the thermal conductivity.

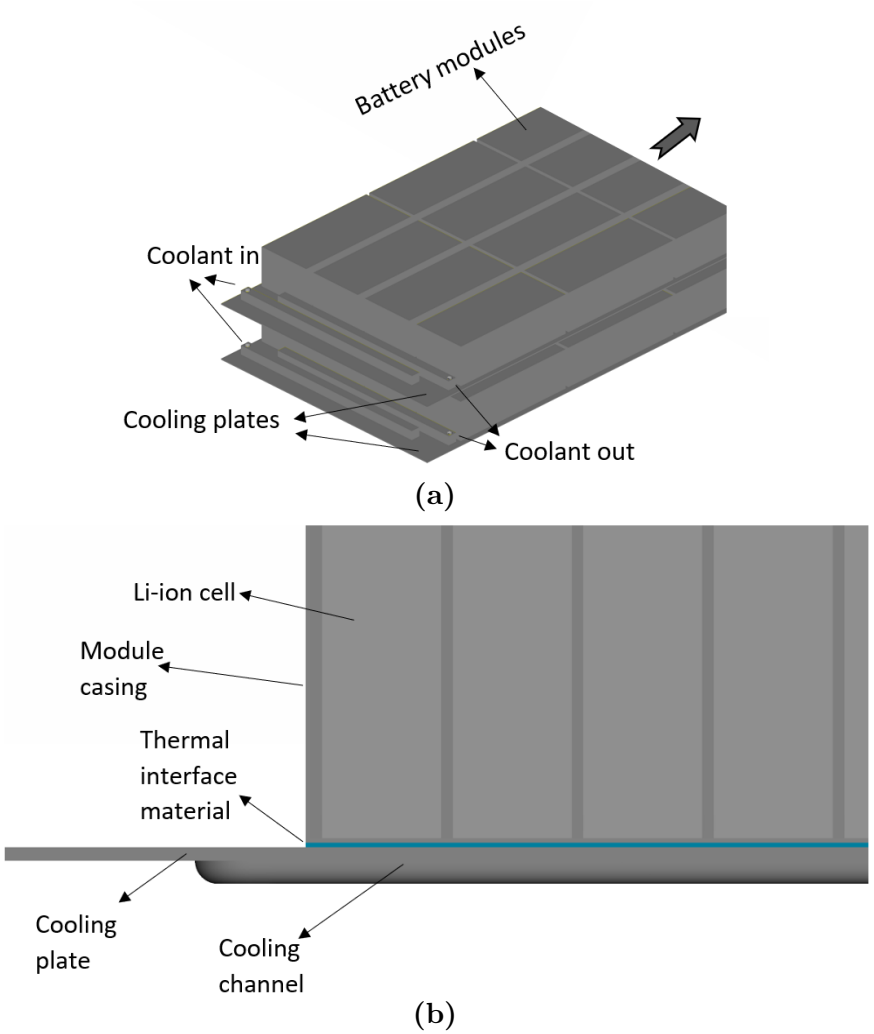

Figure 2.1: *3D representation of the battery pack: (**a**) isometric view; (**b**) Cross-sectional view of the module assembly.*

The conservation equations were discretized using the control volume method on a staggered grid. The transient simulations were solved implicitly with a timestep size 0.1 s. The scalar and vector quantities are solved only in the direction of fluid flow. In order to couple the heat transfer between the fluid and solids, the heat transfer coefficient (h) must be estimated. Since the flow is not resolved in the wall normal direction, the heat transfer coefficient between the wall of the cooling channel and coolant was calculated using an analytical heat transfer correlation for internal convection. It is worth mentioning that several analytical correlations available in GT-SUITE were tested and they all produced very similar results. Colburn analogy [65], as seen in eqn. 2.4, was chosen due to its wide usage and straightforward implementation.

$$j_{th} = \frac{Nu_D}{Re_D Pr^{1/3}} \tag{2.4}$$

where j_{th} is the j-factor, Nu_D and Re_D are the Nusselt and Reynold's numbers, respectively,

based on the channel's diameter and Pr is the Prandtl number.

For pipe flows, the values of j_{th} are typically around $C_f/2$ [66], where C_f is the Fanning friction factor and defined for laminar flows (Re_D <2000) [65] as:

$$C_f = \frac{16}{Re_D} \tag{2.5}$$

Hence, after computing the Reynold's number for the cooling channel, the j-factor and the heat transfer coefficient were estimated.

The heat transferred (Q) between the coolant and the cooling plate was then computed as:

$$Q = hA_c(T_w - T_f) \tag{2.6}$$

where A_c is the surface contact area between the cooling plate wall and the coolant, T_w is the surface temperature of the cooling plate and T_f is the bulk coolant temperature.

The coolant's volumetric flow rate and temperature were imposed at the inlet. The pressure at the outlet was set to match the measured data. The Neumann boundary condition was applied for the fluid temperature at the outlet, i.e $\frac{\partial T}{\partial x} = 0$.

The battery pack was discretized at the module level. Each battery module was represented as a single thermal mass. The consequence is that all cells in the battery module have the same temperature. This assumption holds good for relatively low C-rates when the cell temperatures are approximately constant.

The battery modules were in contact with the module casing and heat transfer between the two was modelled through conduction. Each cooling plate was discretized into 20 lumped thermal masses and they were thermally connected with each other to account for conduction. The temperature of each lumped mass at any instant is calculated using the expression:

$$\dot{Q}_{net} = mc_p\frac{dT}{dt} \tag{2.7}$$

where $\dot{Q}_{net}$ is the net rate of heat accumulation in the lumped mass, m is its mass, c_p is the specific heat capacity of the material and $\frac{dT}{dt}$ is the rate of change of temperature of the lumped mass.

The thermal interface material present between the module casing and the cooling plate was modelled using thermal resistance where the thickness and the thermal conductivity of the interface material, which were unknowns, could be represented as one variable. The thermal resistance of the interface to the transfer of heat was then given by:

$$R_{th} = \frac{t_{TIM}}{kA_c} \tag{2.8}$$

where t_{TIM} is the thickness of the thermal interface material.

Property/Material	Aluminium	Stainless Steel	Coolant	Li-ion battery
Density (kg/m^3)	2702	7900	1057	1827
Thermal conductivity (W/mK)	237	14.9	0.423	19.3
Specific heat (J/kgK)	903	477	3484	1145
Dynamic viscocity (Pa/s)	-	-	0.0023	-

Table 2.1: *Physical properties of the materials in the battery pack used in the model.*

Finally, the battery casing, made of stainless steel, was modelled as a separate thermal mass. Table 2.1 shows the properties of the materials used in the battery pack.

In Paper-A, Bernardi's model of heat generation [20] was used to estimate the heat generated (Q) from each module which reads:

$$Q = N_{mod}\left(I^2 R_{int} + IT\left(\frac{dU_{oc}}{dT}\right)\right) \tag{2.9}$$

where $\dot{Q}$ is the heat generated, N_{mod} is the number of cells in a module, I is the current, R_{int} is the internal resistance of the cells in the module, T is the temperature of the battery module and $\frac{dU_{oc}}{dT}$ is the entropic coefficient. R_{int} and $\frac{dU_{oc}}{dT}$ were obtained based on measurements performed on the battery pack.

The first term on the right hand side of the equation 2.9 is the heat generated due to irreversible ohmic loss and the second term on the right is due to reversible entropic heat loss. R_{int} is a function of the temperature of the module and state of charge (SoC), and $\frac{dU_{oc}}{dT}$ is a function of SoC. These quantities were interpolated accordingly during the simulation. The SoC of the battery pack was estimated in the model as:

$$SoC = SoC_0 + \frac{1}{C}\int_0^t \eta_b I dt \tag{2.10}$$

where SoC_0 is the initial SoC, C is the capacity of the battery and η_b is the efficiency of the battery.

In Paper-B, a second-order Thevenin electrical circuit model (ECM) [67] was used to describe the electrical behaviour of the cells together with the Bernardi's thermal model [20] to account for heat generation. The ECM uses resistors (R_i) and capacitors (C_i) to estimate the output voltage. The schematic of the ECM is illustrated in Fig. 2.2. The output voltage (V) is computed as [68]:

$$U_i(k+1) = U_i(k)e^{-\frac{\Delta t}{R_i C_i}} + R_i(1 - e^{-\frac{\Delta t}{R_i C_i}})I(k) \tag{2.11}$$

where i takes the values [1,2] for the corresponding RC branch and,

$$V(k) = U_{oc}(SoC(k)) - U_1(k) - U_2(k) - R_0 I(k) \tag{2.12}$$

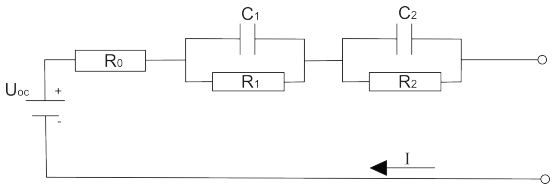

Figure 2.2: *Schematic of the second-order Thevenin electrical circuit model.*

where Δt is the timestep size, k is the timestep number, U_i is the voltage drop across the i^{th} RC branch.

Look-up tables as functions of current, battery temperature and SoC were created for the model parameters R_0, R_1, R_2, C_1 and C_2 by using the experimental measurements. The ECM was also discretized at the module level. All battery cells within the same module were assumed to have identical states.

Heat transfer calibration[1]

Battery module - Coolant

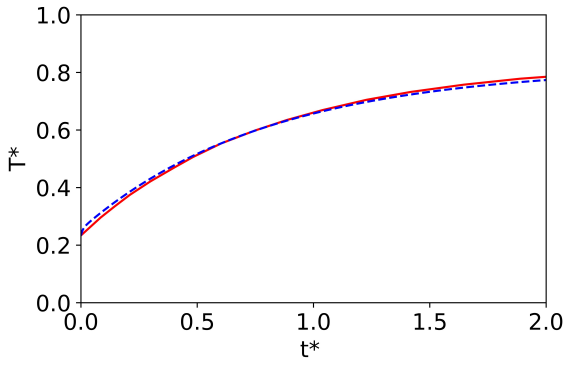

Figure 2.3: *Average battery pack temperature during the heat-up test: Measured* ——, *simulated* - - - -.

The resistance of the thermal interface material is often an unknown quantity while modelling a battery pack as this information is withheld by the battery supplier. For this reason, data from the heat-up test of the battery pack were used to estimate its value. The battery pack with the initial temperature of $0.233T^*$ (where $T^* = T/T_{ref}$ and T_{ref} is an arbitrarily chosen reference temperature) was heated by the coolant at $0.833T^*$ flowing at $0.8Q^*$ (where $Q^* = Q/Q_{ref}$ and Q_{ref} is an arbitrarily chosen reference volume flow rate) and the average pack temperature was measured. The battery pack was inactive and so there was no heat generated from it. The thermal resistance was optimized in the model using the Nelder-Mead optimization approach [69] with the objective to minimize the difference between the experimental and simulation values for the average

[1]The quantities in this section have been non-dimensionalized/hidden due to confidentiality reasons

pack temperature. Figure 2.3 shows the comparison between measured and simulated temperature profiles for the heat-up test.

Battery module - Ambient

Similarly, the heat transfer between the modules and the battery pack casing was modelled using a thermal resistance. The thermal resistance between the battery modules and the battery casing was calibrated using the temperature measurement data from a cool-down test of the battery pack. In this test, the battery pack initially at $0.66T^*$, was allowed to cool down at an ambient temperature of -$0.5T^*$ and the average battery pack temperature was monitored. The thermal resistance was optimized using the Nelder-Mead optimization approach [69] so that the difference between the simulated and the measured temperature values was minimized. Figure 2.4 illustrates the agreement between the measured and simulated average battery pack temperatures during cool-down.

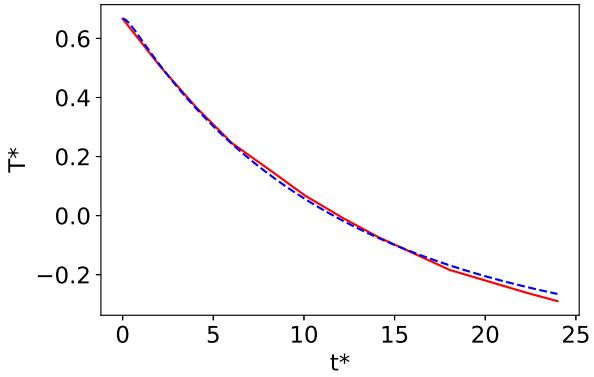

Figure 2.4: *Average battery pack temperature during the cool-down test: Measured* ——, *simulated* - - - -.

2.2 Battery pack model validation

In Paper-A, the developed battery pack model was validated using the experimental data from four test scenarios. Only the thermal model was used in this paper. Two of the studied cases (Case-1 and Case-4) are discussed here.

Case 1 represents a discharging/charging cycle. Figure 2.5 illustrates the pack operation under Case 1 scenario. The transient current profile (Fig. 2.5a) shows that the C-rates (current relative to the nominal battery capacity) are varied between -1.5 C and 1 C followed by a constant current charging at 0.5 C. The volumetric flow of the coolant was kept nearly constant at the inlet and a small variation in its temperature was observed as shown in Fig. 2.5b.

It should be noted that the step profile in the measured temperature values in Fig. 2.6a is due to the resolution of the sensors used during the measurements. The sensors used for the measurement of the average pack temperature were provided by the battery suppliers

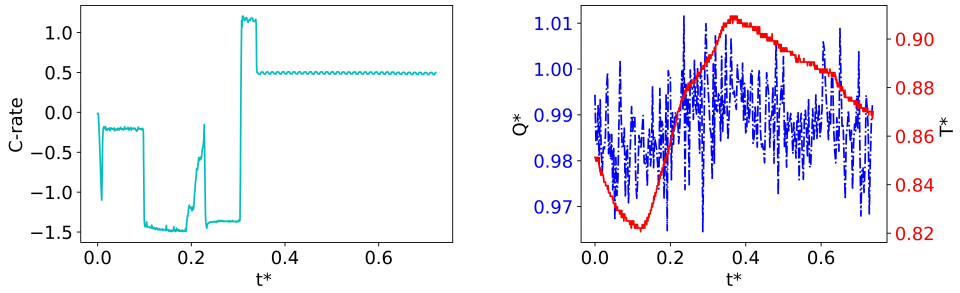

(a) (b)

Figure 2.5: *Case-1 test scenario: (a) Current profile* — *and (b) Inlet volumetric flow rate (Q^*)* - - - - *and temperature of the coolant (T^*)* —.

and hence could not be accessed or modified. Nonetheless, the average temperature of the battery pack predicted by the simulations is in good agreement with the measurements. The average battery pack temperature was predicted well both during discharging ($t^* \leq 0.3$) and charging ($t^* \geq 0.4$) but slightly under-predicted during the transition from discharging at -1.5 C to charging at 1 C ($0.3< t^* <0.4$). The temperature of the coolant at the outlet and the average SoC of the battery pack were estimated well from the simulation as seen in Fig. 2.6b and Fig. 2.6c respectively.

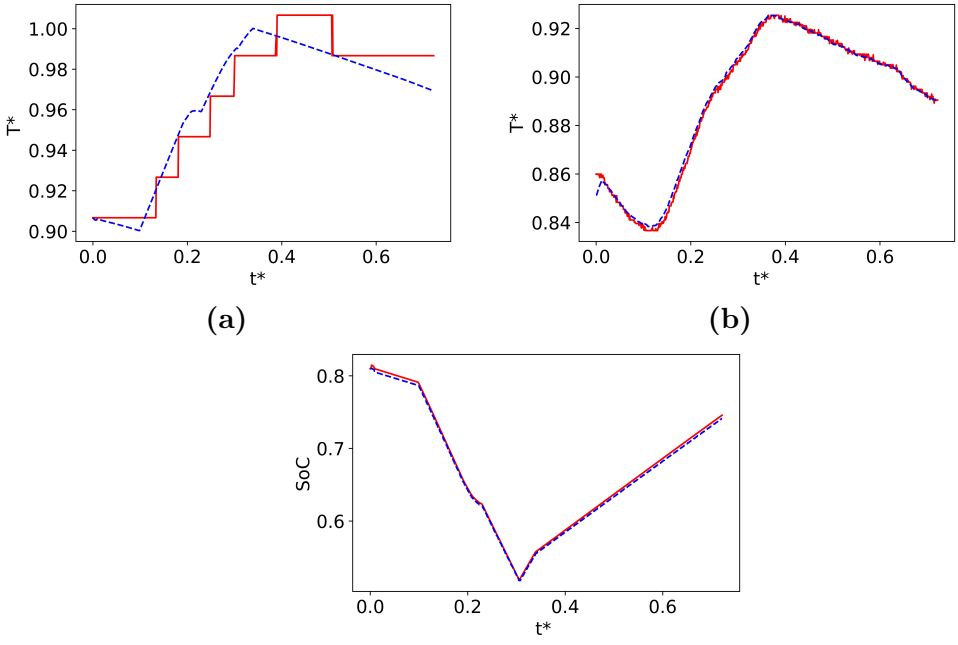

(a) (b)

(c)

Figure 2.6: *Results for Case-1: (a) Average battery pack temperature, (b) Outlet coolant temperature and (c) Average battery pack SoC . Measured* —, *simulated* - - - -.

Case 4 depicts a cooling scenario when the battery pack is not operating (Fig. 2.7a). Here, the coolant flow rate at the inlet was decreased gradually throughout the cycle by decreasing the power of the pump, as the temperature of the battery pack decreased. This is reflected in the coolant's temperature at the inlet as well, see Fig. 2.7b.

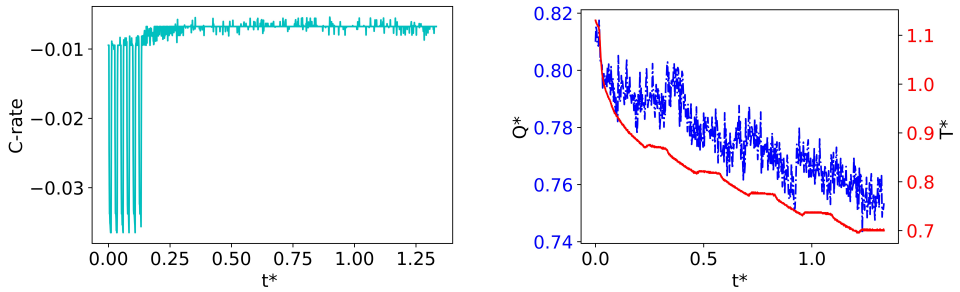

(a) **(b)**

Figure 2.7: *Case-4 test scenario: (a) Current profile* —— *and (b) Inlet volumetric flow rate (Q^*)* - - - - *and temperature of the coolant (T^*)* ——.

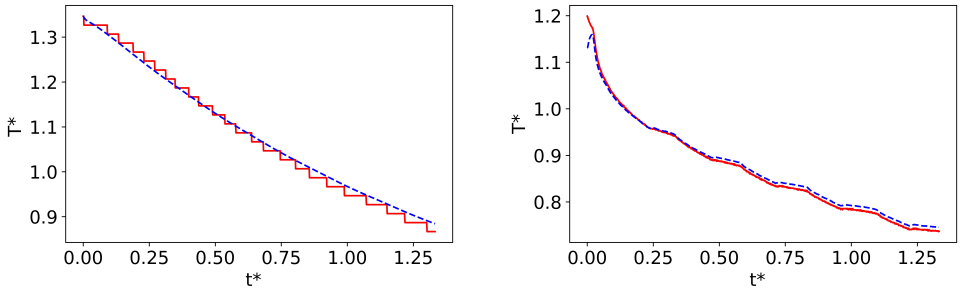

(a) **(b)**

Figure 2.8: *Results for Case-4: (a) Average battery pack temperature and (b) Outlet coolant temperature. Measured* ——, *simulated* - - - -.

The results for Case 4 that represents cool down of the battery pack with continuously decreasing coolant volumetric flow rate are shown in Fig. 2.8. The variations in the average pack temperature are due to heat rejection from the pack to the coolant. The average temperature of the battery pack and the outlet temperature of the coolant were marginally over-predicted in the simulations as compared to the measurements.

The root mean square (RMS) errors in the estimation of the average battery pack temperature, the outlet coolant temperature and the SoC of the battery pack are presented in Table 2.2. As it was seen from the plots, the error in estimation was slightly higher when the current profile and/or flow rate varied. Nevertheless, the magnitude of error is very low and in the order of the resolution of the sensors used.

The transient profiles of the battery pack temperatures and the coolant outlet temperatures were estimated very well for Cases 1 and 3 which had nearly steady conditions for coolant

Case	Average battery pack temperature (K)	Outlet coolant temperarture (K)	SoC (%)
1	0.3291	0.0486	0.338
2	0.5474	0.1708	0.284
3	0.2405	0.0508	0.270
4	0.3576	0.2561	-

Table 2.2: *RMS errors between simulated and measured quantities for the four cases.*

flow. Minor discrepancies were however observed for Cases 2 and 4 with dynamic coolant flow rates and temperature. These deviations can be attributed to the usage of empirical models for heat generation in the battery and heat transfer between the coolant and the wall. While these empirical models perform well in steady-state operating conditions, small deviations arise when the conditions are dynamic. Nevertheless, the overall prediction of the quantities is still in good agreement with the measurements. The modeling framework relies on simplifying the physics to capture the important underlying features of the battery pack. More information about the other cases (Case-2 and Case-3) used for model validation and some other characteristics of the modeling strategy are discussed in Paper-A [1].

In Paper-B, the ECM was validated for three cyclic charge-discharge current profiles. The simulation results for the battery pack voltage were compared with the experimental measurements. The current profiles had a maximum current of 2 C during charge and discharge, and they each varied in frequency as shown in Fig. 2.9. The root mean square (RMS) error was computed for the three cases (see Table 2.3). The ECM marginally under-predicted the average battery pack voltage with the maximum RMS error of 1%.

Case-1	**Case-2**	**Case-3**
0.567%	0.699%	0.973%

Table 2.3: *RMS error of the normalized battery pack output voltage.*

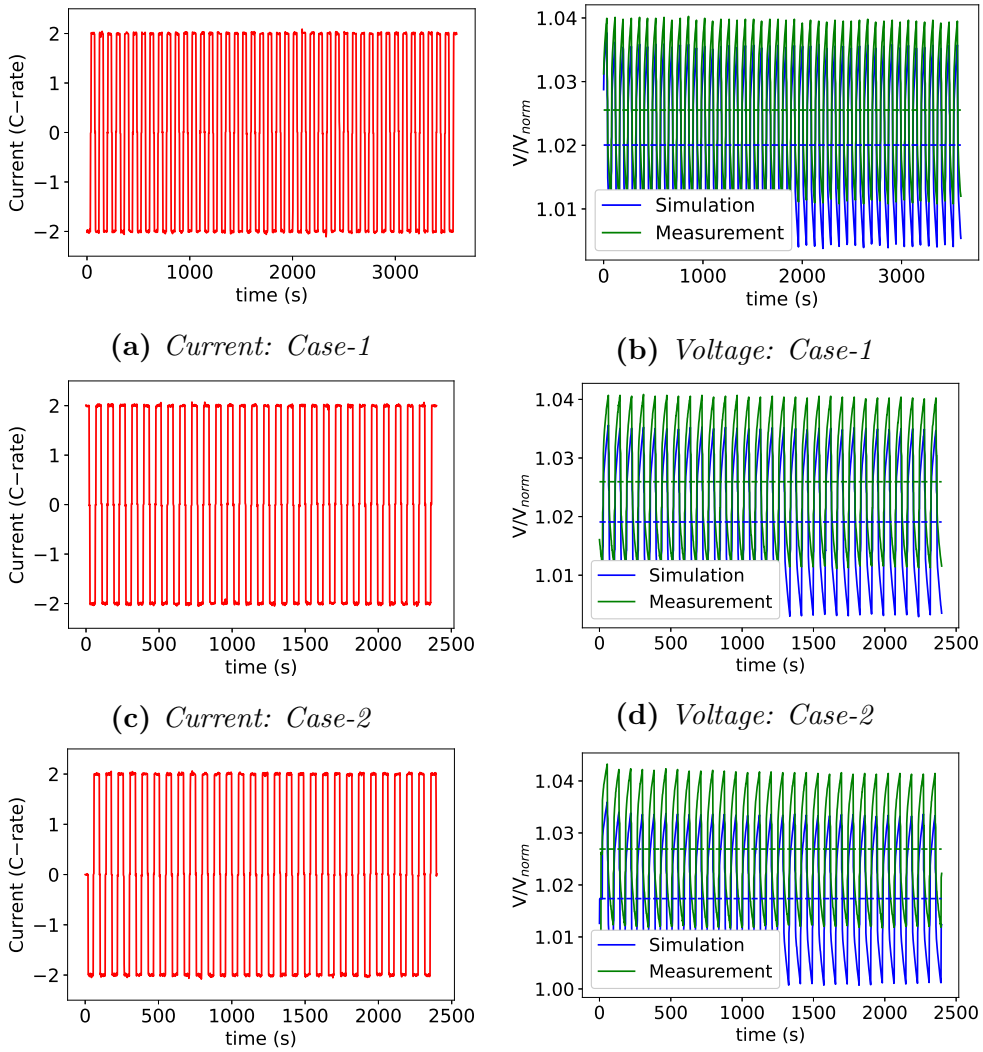

(a) *Current: Case-1*

(b) *Voltage: Case-1*

(c) *Current: Case-2*

(d) *Voltage: Case-2*

(e) *Current: Case-3*

(f) *Voltage: Case-3*

Figure 2.9: *Validation of the Thevenin 2RC model.*

2.3 Vehicle model

In paper-B, a simplified truck model was included in addition to the battery pack. The vehicle considered was a fully electric truck and its main specifications are presented in Table 2.4. Figure 2.10 illustrates a schematic of the simplified truck model used in the work. It had two axles, each driven by an electric motor through a differential. The electric motors served also as generators to regenerate energy while braking. The efficiency map of the electric machine as a function of the operating torque (τ) and speed (ω) is shown in Fig. 2.11. The traction power was calculated as:

$$P_v = \left(M_v a_v + \frac{1}{2} \rho v_v^2 C_d A_{f_v} + \mu_r M_v g cos(\alpha) + M_v g sin(\alpha) \right) v_v \tag{2.13}$$

where M_v is the mass of the vehicle, a_v is the acceleration, ρ is the density of air, v_v is the velocity of the vehicle, C_d is the coefficient of drag, A_{f_v} is the frontal area, μ_r is the rolling resistance coefficient of the tyre, g is the acceleration due to gravity and α is the road gradient.

The electric machines received information about the maximum discharge/charge ability of the batteries during each timestep in the simulation. During braking, the brake controller unit received messages about the maximum power that could be sent to the batteries to be stored and the maximum braking torque the motor could produce. If the regenerated power was lower than the maximum charge threshold, the batteries were charged whereas if the regenerated power exceeded the maximum threshold, the batteries charged at their limits and the rest of the braking torque was supplied by the friction brakes. Finally, the vehicle was driven by a driver model whose input was a prescribed speed profile (drive cycle). The driver model requested torque from the two electric motors to match the actual vehicle speed with the target speed profile. The driver received information about the position of the vehicle to satisfy the total distance travelled as a result of the prescribed speed profile.

Parameter	Value
Vehicle mass (M_v)	15000 kg
Tyre rolling resistance (μ_r)	0.008
Drag coefficient (C_d)	0.5
Frontal area (A_{f_v})	10 m^2
Gear-train efficiency (η_{gt})	0.95

Table 2.4: *Truck specifications.*

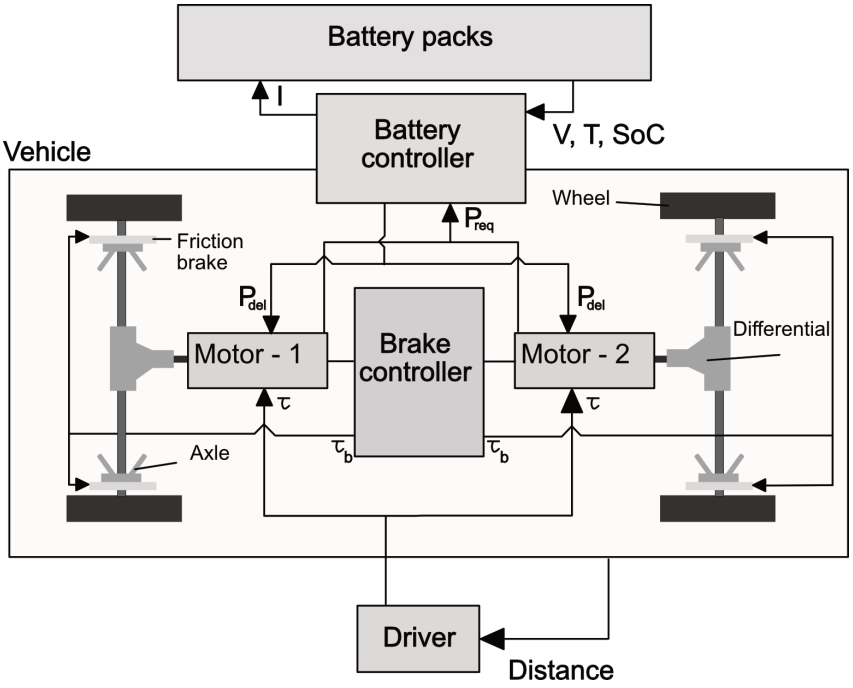

Figure 2.10: *Schematic of the simplified truck model.*

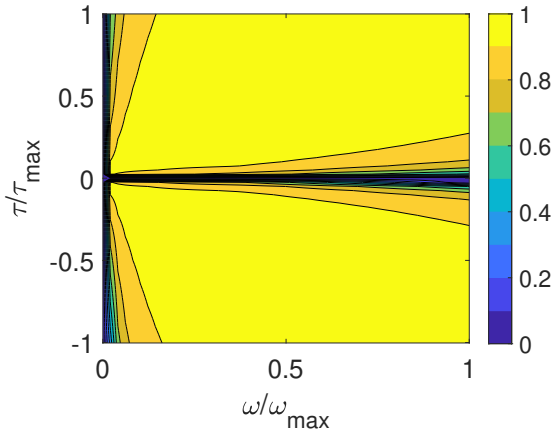

Figure 2.11: *Electric machine efficiency map.*

2.3.1 Battery pack control unit

The simplified control logic for the battery pack simulations is shown in Fig. 2.12. The electrical power was requested/delivered by/from the electric motor-generator unit. This power was then converted to discharge/charge current based on the battery's output voltage. In addition, the battery pack's maximum discharge/charge ability in terms of power was considered as threshold and was represented as a function of temperature and SoC as seen in Fig. 2.13a and Fig. 2.13b, respectively. When the coolant heaters were engaged to heat up the battery packs, this power demand was also considered in addition

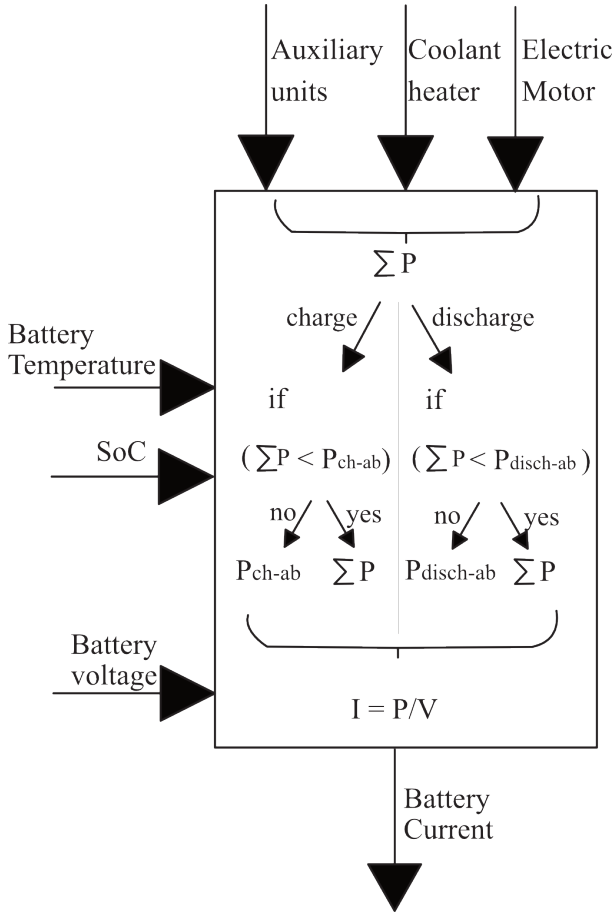

Figure 2.12: *Battery pack control logic.*

to the request from the traction components and the auxiliary units.

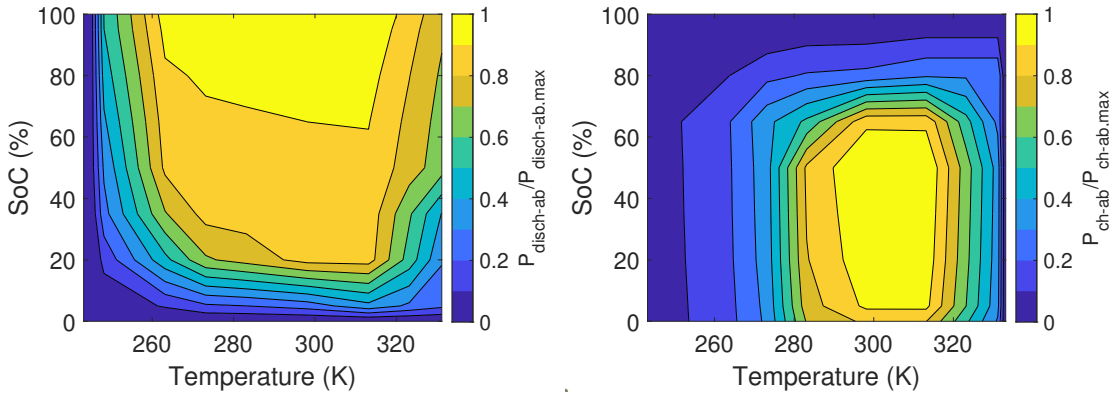

(a) *Normalized battery discharge ability as a function of SoC and temperature.*

(b) *Normalized battery charge ability as a function of SoC and temperature.*

Figure 2.13: *Battery performance.*

2.3.2 Energy storage cooling system

The schematic of the cooling system for the electric energy storage is presented in Fig. 2.14. A pump was used to provide cooling for the three battery packs. A 2.5 kW coolant heater was placed in front of each battery pack to supply heat in case their temperatures fell below a threshold value. The ideal battery operating temperature range is 15°C to 35°C [70, 71] and therefore the threshold temperature was set to 15°C. The radiator bypass valve was used to regulate the coolant flow through the radiator. In the cases that either the coolant heaters were engaged or the average temperature of the packs fell below 25°C, the flow was bypassed from the radiator whereas if the temperature of the battery packs was above 25°C, the bypass valve was shut off and the coolant flowed through the radiator.

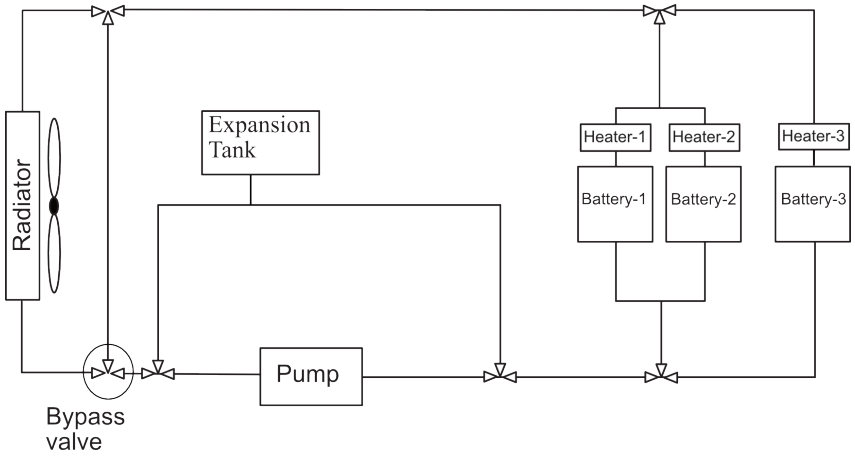

Figure 2.14: *Schematic of the electric energy storage cooling circuit.*

The presented framework can be used to perform vehicle drive cycle simulations while capturing the electrical-thermal performance of the battery pack. In the next chapter, the performance of the battery pack under different operating temperatures, and the effect of battery pack encapsulation on the vehicle energy consumption are analyzed.

3

Effects of battery pack encapsulation

The vehicle considered, had three battery packs which were modelled as described in the previous chapter. All the battery packs were encapsulated using thermally insulating materials as seen in Fig. 3.1. Plates of insulation with a certain thickness and material properties were placed on each side of the battery pack. The thermal conduction between the battery pack casing and the thermal insulation was considered. The net increase in the truck's total mass due to the presence of the insulating material was taken into account when calculating the power request. In this chapter, the battery packs without thermal encapsulation were also considered and referred to as the baseline configuration.

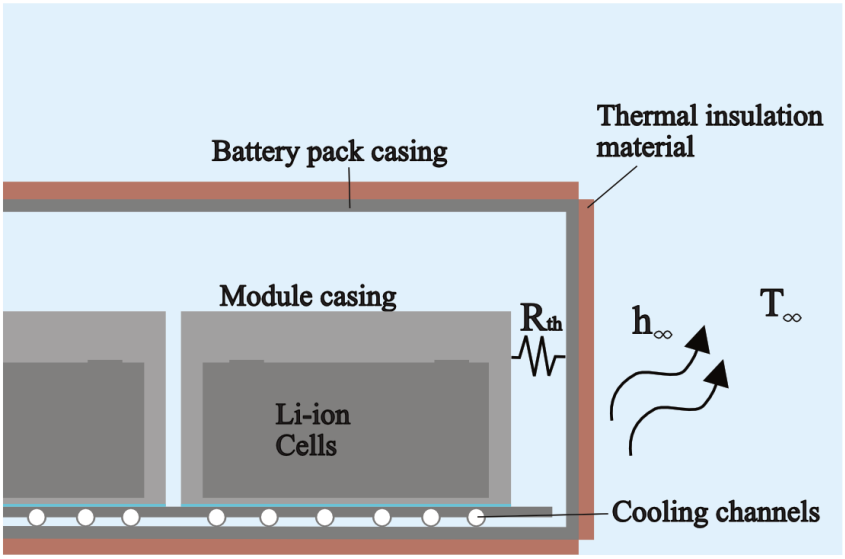

Figure 3.1: *Thermal encapsulation of the battery pack.*

3.1 Simulation methodology

To capture the vehicle and battery pack performance, a transient drive cycle was used and the EPA's highway fuel economy test (HWFET) was chosen for this purpose (see Fig. 3.2). The power required to drive the truck at this imposed speed is given by eqn. 2.13. The simulations were performed to investigate:

1. Temperature influence of the battery pack performance
2. Influence of battery pack encapsulation on parking-driving scenarios at different ambient temperatures
3. Parametric analysis of encapsulation characteristics

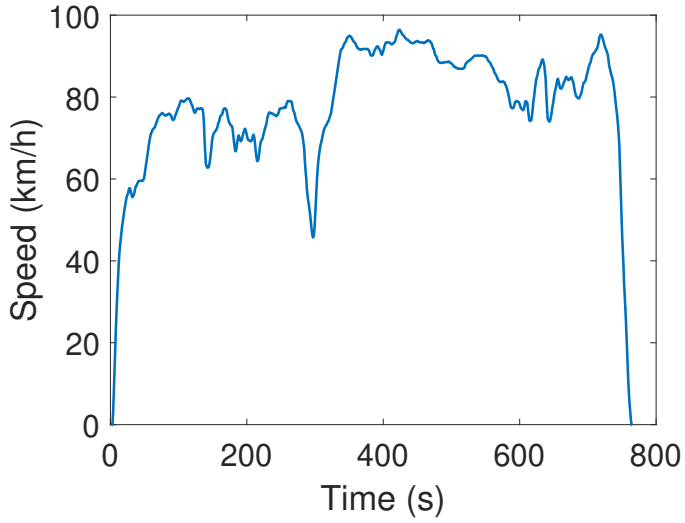

Figure 3.2: *EPA HWFET drive cycle; Duration - 765 s; Distance - 16.45 km; Average speed - 77.7 km/h [72].*

In all the simulations, the initial SoC for the battery packs was 80%.

3.1.1 Temperature influence on the battery pack performance

Five different initial pack temperatures, 40°C, 25°C, 10°C, 0°C and -10°C were considered to assess the performance of the battery pack in the baseline configuration. The coolant heaters were not used in this study. The voltage output from the battery pack, the current requested/delivered and the average energy consumption during the drive cycle were analyzed.

3.1.2 Influence of battery pack encapsulation on parking-driving scenarios at different ambient temperatures

A parking-driving scenario consisting of a 12-hour parking period followed by five consecutive HWFET cycles was considered as seen in Fig. 3.3. The simulations were performed at five ambient temperatures, 25°C, 10°C, 0°C, -10°C and -25°C, with the initial battery pack temperature at 25°C. The coolant heaters were engaged to heat the battery packs when the driving phase started. As previously mentioned, the coolant heaters were turned on when the battery pack temperatures were below 15°C. Both the baseline configuration and the encapsulated battery packs were examined. The information about the encapsulation

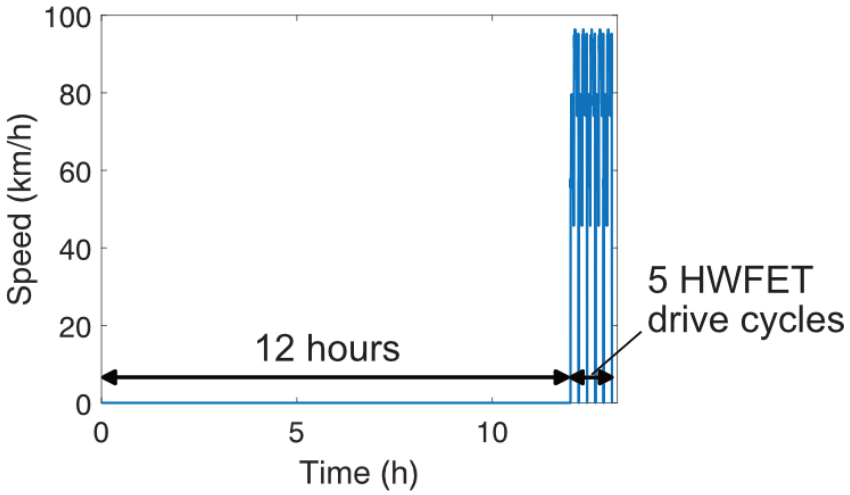

Figure 3.3: *Parking-driving cycle.*

Property	Value	Unit
Encapsulation thickness (t)	0.0127	m
Thermal conductivity (k)	0.027	W/mK
Density (ρ)	61	kg/m^3
Specific heat (c_p)	2500	J/kgK

Table 3.1: *Battery pack encapsulation characteristics.*

thickness and the properties of the commercially available insulating material are presented in Table 3.1.

3.1.3 Parametric analysis of encapsulation characteristics

Finally, the encapsulation thickness and the material properties of the encapsulation material (see Table 3.2) were varied to analyze their effects on the pack's performance in cold climates. Three ambient temperatures, 0°C, -10°C and -25°C were considered and the same parking/driving scenario was simulated as presented in Fig. 3.3. Only one property was varied at a time. The variation in the truck's mass due to changes in the

Property	Values
Encapsulation thickness (m)	0.00635, 0.0127, 0.0254, 0.0508
Thermal conductivity (W/mK)	0.001, 0.01, 0.1, 1
Density (kg/m^3)	30, 60, 120, 240, 480
Specific heat (J/kgK)	500, 1000, 2000, 4000

Table 3.2: *Sensitivity analysis of the encapsulation thickness and material properties of the insulating material.*

encapsulation mass (material density and encapsulation thickness) was considered when calculation traction power. The battery pack temperature at the end of the parking phase, the energy consumed by the coolant heaters, the average energy consumption during the drive cycle and the percentage of energy savings relative to the baseline configuration were used to assess the performance of each design configuration. The results are categorized based on the thermal resistance ($R_{th} = t/k$) and thermal capacitance ($C_{th} = \rho c_p$) of the encapsulation.

3.2 Results and discussion

Figure 3.4 shows an excellent agreement between the target and the simulated speed when the truck is run through the HWFET drive cycle. Based on the driver's torque request from the electric motors, and the electric motors' power request from the batteries, the target vehicle speed is achieved.

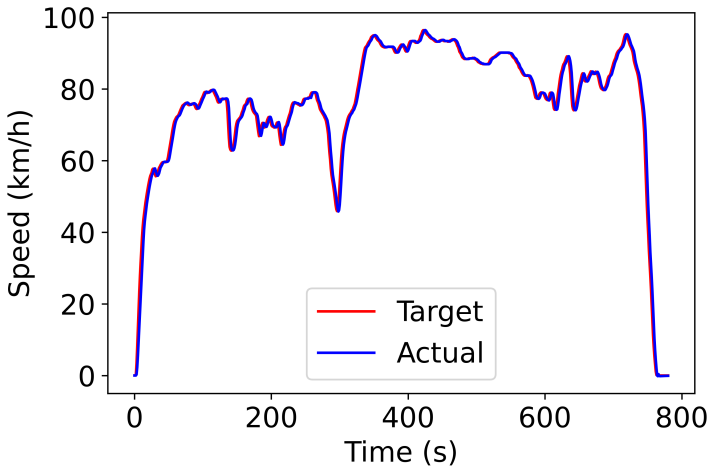

Figure 3.4: *A comparison between the target and simulated speed of the truck under the HWFET drive cycle.*

3.2.1 Temperature influence of the battery pack performance

Figures 3.5a and 3.5b present the variations in the output voltage and discharge/charge currents respectively, during the HWFET drive cycle. Note that the negative values represent discharge currents and positive values, charge currents.

A decrease in the output voltage is observed with a decrease in the battery pack temperature. The output voltage is a function of the internal battery resistance. A decrease in the operating temperature leads to an increase in the internal resistance which results in lower output potential. Consequently, higher discharge currents are required at lower operating temperatures (see Fig. 3.5b). At the same time, the charging ability of the batteries during regenerative braking is reduced at these temperatures (see Fig. 2.13b). Thus, the

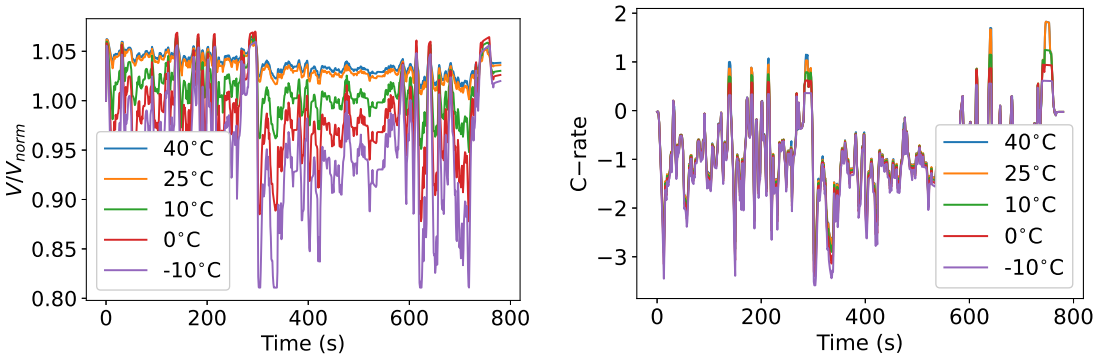

(a) *Output voltage from the battery pack for HWFET drive cycle at different operating temperatures.*

(b) *Current requested from/delivered to the battery pack at different operating temperatures.*

Figure 3.5: *Battery performance during the EPA HWFET cycle.*

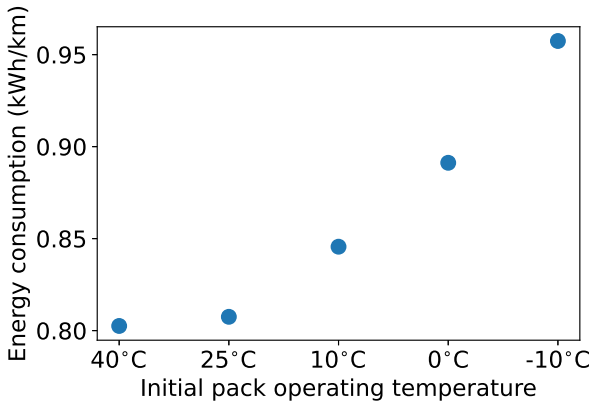

Figure 3.6: *Average truck energy consumption during the HWFET driving cycle for different pack operating temperatures.*

battery discharges more and recovers lesser energy while operating at low temperatures. Figure 3.6 illustrates the relationship between the average energy consumption of vehicle and the battery pack operating temperature during the HWFET drive cycle. An increase in the average energy consumption with a decrease in temperature is seen for the operating temperatures below 25°C. The battery pack consumes an average of 0.15 kWh/km (18.7%) more at -10°C as compared to the pack operating at 25°C.

3.2.2 Influence of battery pack encapsulation on parking-driving scenarios at different ambient temperatures

The average battery pack temperatures under parking-driving scenario at different ambient temperatures are presented in Fig. 3.7a. The battery pack temperature was initialized to 25°C. The horizontal black dotted line represents the 15°C temperature threshold for battery pack heating during its operation. It is observed that the encapsulated battery

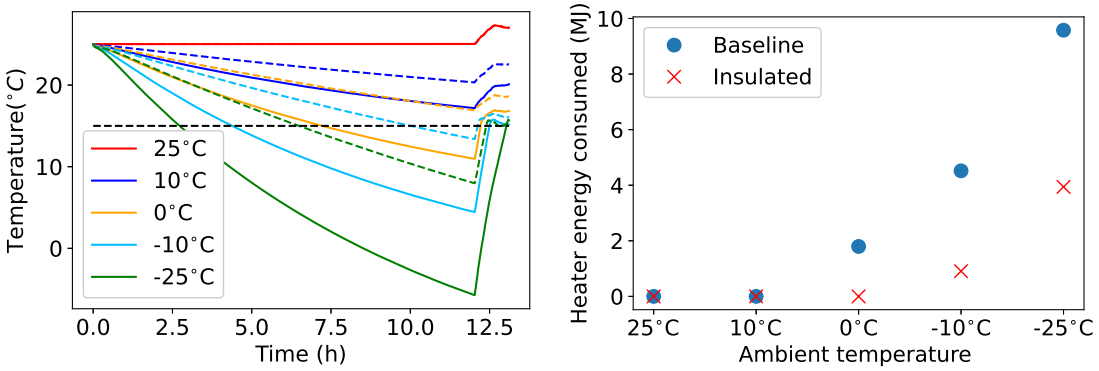

(a) *Average battery pack temperature; Baseline configuration (−), Encapsulated configuration (−−).*

(b) *Energy consumed by the coolant heater to heat up the battery pack.*

Figure 3.7: *Comparison between baseline vs encapsulated pack.*

pack retains higher temperatures (dotted lines) compared to the baseline configuration (solid lines) at all ambient temperatures except 25°C where the initial pack and ambient temperatures are equal.

The energy provided by the coolant heater to heat the battery pack at different ambient temperatures is shown in Fig. 3.7b. The energy consumed by the coolant heaters increases for both the encapsulated and the baseline configurations for the ambient temperatures -10°C and -25°C. However with battery pack encapsulation, the requirement is reduced. At 0°C, the encapsulation acclimatizes the battery pack above the 15°C threshold, thereby eliminating the need for heating. Figure 3.8 and Table 3.3 illustrate the average truck energy consumption during the driving phase and the percentage of energy saved with the encapsulated configuration relative to the baseline configuration, respectively. At 25°C, the energy consumed is marginally (0.03%) higher for the encapsulated configuration due to the increased truck mass. Nevertheless, the average energy consumption for the

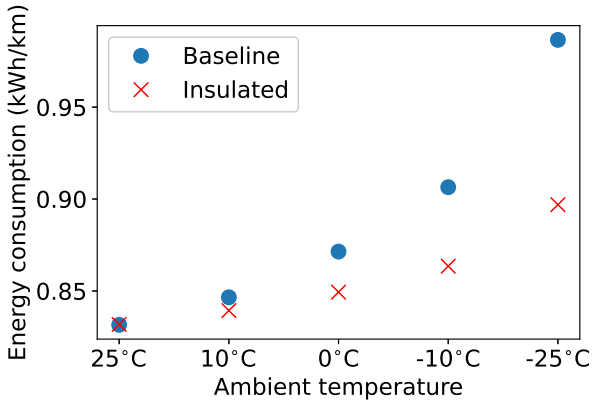

Figure 3.8: *Average vehicle energy consumption during the parking-driving scenario.*

Ambient temperature (°C)	Energy saving (%)
25	-0.03
10	0.85
0	2.53
-10	4.74
-25	9.08

Table 3.3: *Percentage of energy savings with the encapsulated pack relative to the baseline configuration at different ambient temperatures.*

encapsulated pack is lower than the baseline pack at all low ambient temperatures (10°C, 0°C, -10°C and -25°C). The combined effects of higher pack operating temperature and reduced energy expenses for the coolant heaters are responsible for the outcome. The energy saved increases for the encapsulated configuration with a decrease in ambient temperature to approximately 9% at -25°C.

3.2.3 Parametric analysis of the encapsulation characteristics

Effects of variation in the encapsulation's thermal resistance

The thickness and thermal conductivity of the encapsulation relate to the thermal resistance of the material. These quantities were varied as specified in Table 3.2. Figure 3.9a displays the average temperature of the battery pack at the end of the 12-hour parking period. As expected, a high thermal resistance of the encapsulation results in a battery pack temperature closer to the value at the beginning of the parking phase. With a decrease in the resistance, the pack temperature also reduces as more heat is rejected through the

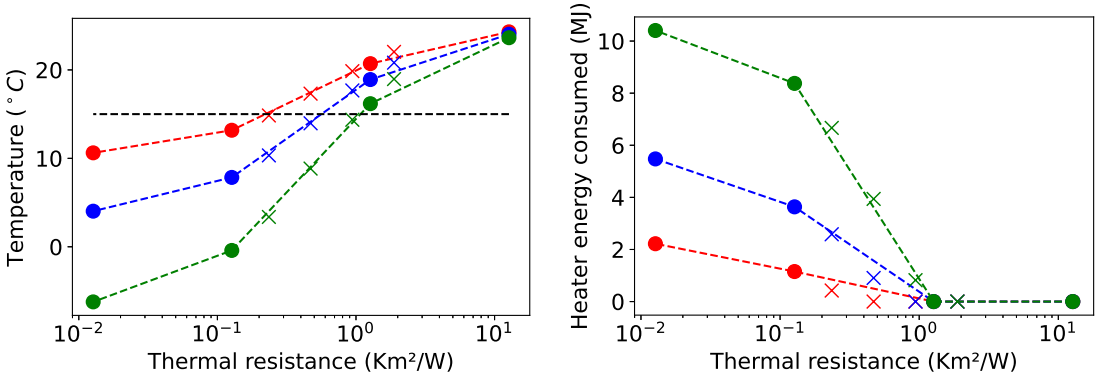

(a) **(b)**

Figure 3.9: *(a) Average battery pack temperature at the end of the 12-hour parking period with variation in the encapsulation resistance; (b) Coolant heaters energy usage during the driving phase with variation in the encapsulation resistance;* •*: variation of k;* ×*: variation of t;* - - - -*:* T_∞*=0°C;* - - - -*:* T_∞*=-10°C;* - - - -*:* T_∞*=-25°C.*

casing and the encapsulation to the ambient.

The variations in the energy consumed by the coolant heater with variations in the encapsulation resistance are shown in Fig. 3.9b. It can be seen that for a thermal resistance of approximately 1 Km^2/W and above, the pack temperature stays above the 15°C threshold value, and hence the heaters are not engaged. However below 1 Km^2/W, with decrease in the thermal resistance, the heat energy consumed increases. The consequence of these effects coupled with the improved battery's performance at higher temperatures results in a decrease in the average energy consumption of the vehicle with increasing thermal resistance of the encapsulation as seen in Fig. 3.10a. The decrease in the average energy consumption with the increase in thermal resistance was found to be asymptotic in nature where further increase in the thermal resistance would result in values closer 0.83 kWh/km which corresponds to the average energy consumption at 25°C (see Fig. 3.8).

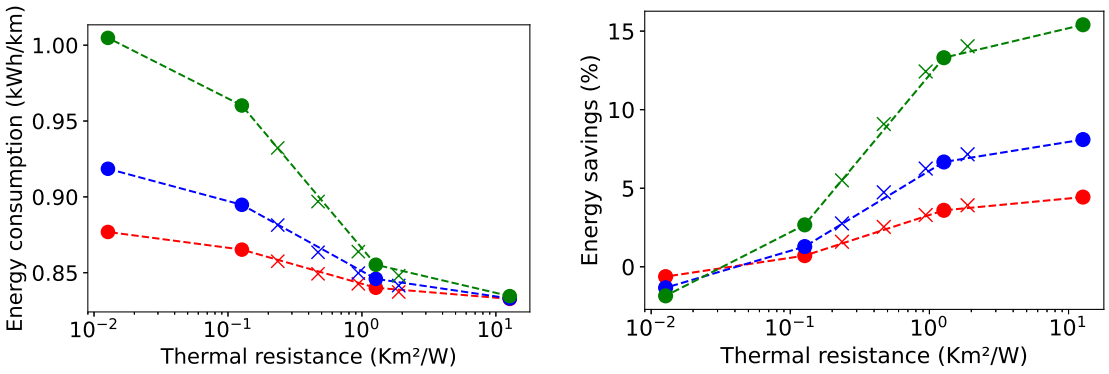

(a) **(b)**

Figure 3.10: *(a) Average vehicle energy consumption during the parking-driving scenario with variation in the encapsulation resistance; (b) Percentage of energy savings with variation in the encapsulation resistance relative to the baseline configuration;* ●*: variation of k;* ×*: variation of t;* - - - *:* T_∞*=0°C;* - - - *:* T_∞*=-10°C;* - - - *:* T_∞*=-25°C.*

Finally, the potential energy savings that can be achieved with encapsulation relative to the baseline configuration in presented in Fig. 3.10b. It can be seen that the energy savings increase with decrease in the ambient temperature and with increase in the thermal resistance of the encapsulation. The thermal resistance of approximately 1 Km^2/W produces energy savings of approximately 3%, 6% and 12% at 0°C, -10°C and -25°C, respectively and beyond that, the savings are asymptotic. Hence, choosing a material with high thermal resistance becomes crucial when operating battery packs at low ambient temperatures.

Effects of variation in the encapsulation's thermal capacitance

The material properties, the density and the specific heat, can be related to the thermal capacitance (or thermal energy stored) of the material. The quantities were varied as

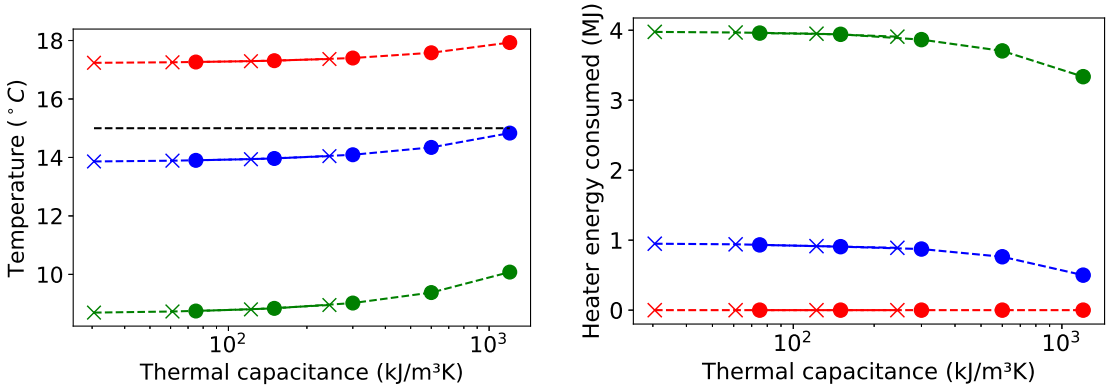

(a) **(b)**

Figure 3.11: *(a) Average battery pack temperature at the end of the 12-hour parking period with variation in the encapsulation capacitance; (b) Coolant heaters energy usage during the driving phase with variation in the encapsulation capacitance; •: variation of ρ; ×: variation of c_p; - - - -: T_∞=0°C; - - - -: T_∞=-10°C; - - - -: T_∞=-25°C.*

described in Table 3.2. The average pack temperature at the end of the 12-hour parking period at different ambient temperatures is shown in Fig. 3.11a. It can be seen that the increase in the thermal capacitance of the encapsulation results in a small improvement in the pack temperature at the end of the parking period. The magnitude of temperature rise with increased thermal energy increases with decrease in the ambient temperature. This effect is observed because with increase in the thermal capacitance, higher heat energy is stored in the encapsulating material shielding the battery pack. While it stores higher energy, it still loses heat to the environment. Once, the encapsulation's energy is depleted sufficiently, the pack begins to lose heat. Hence, a higher capacitance aids in delaying the

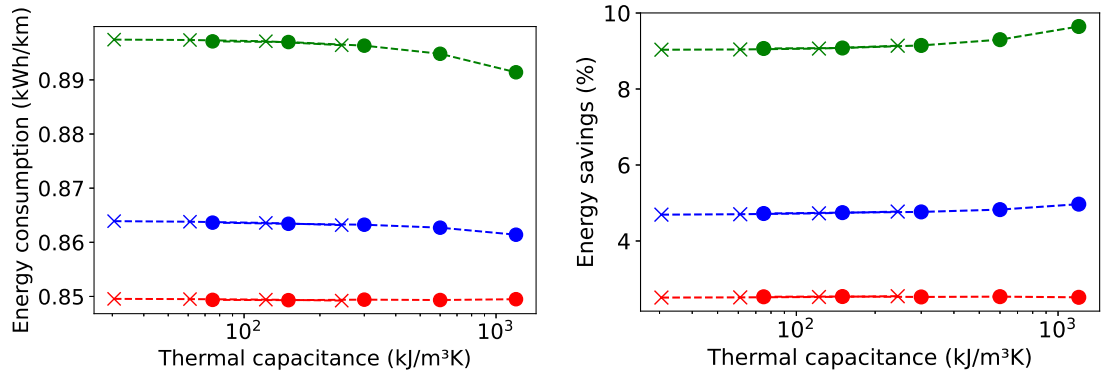

(a) **(b)**

Figure 3.12: *(a) Average vehicle energy consumption during the parking-driving scenario with variation in the encapsulation capacitance; (b) Percentage of energy savings with variation in the encapsulation capacitance relative to the baseline configuration; •: variation of ρ; ×: variation of c_p; - - - -: T_∞=0°C; - - - -: T_∞=-10°C; - - - -: T_∞=-25°C.*

heat loss from the pack. Thus, with higher thermal capacitance, the pack holds a higher temperature at the end of the parking period.

Consequently, the heater energy consumed by the heaters are marginally reduced with increase in the thermal capacitance as seen in Fig. 3.11b. The average vehicle energy consumption and the percentage of energy saved with variations in the thermal capacitance of the encapsulation are presented in Fig. 3.12a and Fig. 3.12b, respectively. Due to the above mentioned effects, a slight decrease in the average energy consumption and increase in energy savings with increase in thermal capacitance are seen.

4

Concluding remarks

The objective of the thesis was twofold. First, to build a battery model that is capable of capturing the dynamic electrical-thermal effects in a battery pack subsystem in conjunction with other vehicle subsystems. Second, to investigate the effect of battery pack encapsulation and its impact on the energy consumption of the vehicle while operating at cold climate.

A 1D module-discretized battery pack model was created to perform electrical-thermal simulations for large packs. The battery pack consisted of two trays where each tray had a cooling plate, thermal interface material, module casing enclosing several Li-ion cells. An electrical circuit model (2RC Thevenin model) was used to capture the electrical characteristics while the Bernardi's thermal equation was used to estimate the heat generation from the modules. The calibrated simulation model was verified using four test scenarios for the thermal model and three cyclic charge-discharge scenarios for the electrical model. The simulation results were in good agreement with the experimental data with a maximum RMS error of 0.55 K in estimating the battery pack temperature, 0.26 K in estimating the outlet coolant temperature, 0.4% in estimating the SoC of the pack and 0.98% in estimating the normalized pack output voltage. These results demonstrate the feasibility of the developed approach for studying the electrical-thermal behaviour of large battery packs. The model provided a good trade-off between model accuracy and speed making it possible to run long simulations.

Along with the developed battery pack model, a vehicle, a cooling system and vehicle controllers were included to perform transient drive cycle simulations. To understand the influence of temperature on the performance of the battery pack, five different battery operating temperatures were simulated under the EPA-HWFET drive cycle. It was noted that the vehicle energy consumption at -10°C was 0.15 kWh/km (18.7%) higher as compared to the consumption at 25°C. This effect was seen due to increased internal resistance of the battery pack at low temperatures leading to higher discharge current coupled with decreased charging ability to regenerate energy during braking. Then, thermal encapsulation in the form of an insulating material with thickness 12.7 mm was added to each side of the battery pack to reduce the rate of cool down. A parking-driving cycle was simulated to study the effectiveness of encapsulation in retaining heat within the battery pack. As expected, the encapsulated battery pack retained a higher temperature

at all low ambient temperatures as compared to the baseline (non-encapsulated) pack. Consequently, the battery's performance improved and the energy used by the coolant heaters reduced leading to decreased energy consumption and an energy saving of about 9% at -25°C ambient temperature. Finally, a parametric analysis on the material properties of the insulating material was performed and it was found that the thermal resistance of the insulating material played a significant role in reducing the heat loss to the environment at low temperatures. An encapsulation thermal resistance of about 1 Km^2/W produced around 3%, 6% and 12% energy savings at 0°C, -10°C and -25°C as compared to a non-encapsulated pack, respectively.

4.1 Future work

It has been shown in the literature that the passenger cabin requires quite a significant amount of energy to be climatized at low ambient temperatures for passenger comfort. The development of a conjugate heat transfer model of a passenger vehicle cabin is underway. This study will aim at investigating the effect of cabin inlet flow rate and temperature, which affect the energy consumption, on the temperature and velocity fields, which affect the comfort of passengers. With this understanding, it is intended to continue using the proposed modeling strategy, results and conclusions of battery pack encapsulation for studies including the cabin and other heat-generating units in BEVs, and investigate methods that are capable of reducing parasitic loads and effectively managing heat demands.

References

[1] Ramesh Babu, A. et al. "System-Level Modeling and Thermal Simulations of Large Battery Packs for Electric Trucks". *Energies* **14**.16 (2021), 4796.

[2] Ramesh Babu, A. et al. "Thermal encapsulation of large battery packs for electric vehicles operating in cold climate". *Submitted to Applied Thermal Engineering* (2022).

[3] BP, B. P. "Statistical Review of World Energy June 2016". *British Petroleum* **201**.6 (2016).

[4] Thakur, A. K. et al. "A state of art review and future viewpoint on advance cooling techniques for Lithium–ion battery system of electric vehicles". *Journal of Energy Storage* **32** (2020), 101771.

[5] "Greenhouse gas emissions from transport. 2019 European Environment Agency". `https://www.eea.europa.eu/data-and-maps/indicators/transport-emissions-of-greenhouse-gases/transport-emissions-of-greenhouse-gases-12`. Accessed: 2022-01-31.

[6] Grigoratos, T. et al. "Real world emissions performance of heavy-duty Euro VI diesel vehicles". *Atmospheric environment* **201** (2019), 348–359.

[7] Andersen, P. H., Mathews, J. A., and Rask, M. "Integrating private transport into renewable energy policy: The strategy of creating intelligent recharging grids for electric vehicles". *Energy policy* **37**.7 (2009), 2481–2486.

[8] Zhang, T. et al. "Status and development of electric vehicle integrated thermal management from BTM to HVAC". *Applied Thermal Engineering* **88** (2015), 398–409.

[9] Minovski, B. "Engine Encapsulation for Increased Fuel Efficiency of Road Vehicles". Chalmers Tekniska Hogskola (Sweden), 2017.

[10] Liu, H. et al. "Thermal issues about Li-ion batteries and recent progress in battery thermal management systems: A review". *Energy conversion and management* **150** (2017), 304–330.

[11] Wang, Q. et al. "A critical review of thermal management models and solutions of lithium-ion batteries for the development of pure electric vehicles". *Renewable and Sustainable Energy Reviews* **64** (2016), 106–128.

[12] Goodenough, J. B. and Park, K.-S. "The Li-ion rechargeable battery: a perspective". *Journal of the American Chemical Society* **135**.4 (2013), 1167–1176.

[13] Fuller, T. F., Doyle, M., and Newman, J. "Simulation and optimization of the dual lithium ion insertion cell". *Journal of the Electrochemical Society* **141**.1 (1994), 1.

[14] Doyle, M. et al. "Comparison of modeling predictions with experimental data from plastic lithium ion cells". *Journal of the Electrochemical Society* **143**.6 (1996), 1890.

[15] Newman, J. and Thomas-Alyea, K. E. "Electrochemical systems". John Wiley & Sons, 2012.

[16] Feng, J., He, Y., and Wang, G. "Comparison study of equivalent circuit model of Li-Ion battery for electrical vehicles". *Research Journal of Applied Sciences* **6**.20 (2013), 3756–3759.

[17] Zhang, H. and Chow, M.-Y. "Comprehensive dynamic battery modeling for PHEV applications". *iEEE PES General Meeting*. IEEE. 2010, pp. 1–6.

[18] Andre, D. et al. "Characterization of high-power lithium-ion batteries by electrochemical impedance spectroscopy. I. Experimental investigation". *Journal of Power Sources* **196**.12 (2011), 5334–5341.

[19] Bandhauer, T. M., Garimella, S., and Fuller, T. F. "A critical review of thermal issues in lithium-ion batteries". *Journal of the Electrochemical Society* **158**.3 (2011), R1.

[20] Bernardi, D., Pawlikowski, E., and Newman, J. "A general energy balance for battery systems". *Journal of the electrochemical society* **132**.1 (1985), 5.

[21] Wang, Z. et al. "Theoretical simulation and modeling of three-dimensional batteries". *Cell Reports Physical Science* (2020), 100078.

[22] Basu, S. et al. "Coupled electrochemical thermal modelling of a novel Li-ion battery pack thermal management system". *Applied Energy* **181** (2016), 1–13.

[23] Saqli, K. et al. "Battery Pack Thermal Modeling, Simulation and electric model Identification". *ICEERE2020 2nd International Conference on Electronic Engineering and Renewable Energy*. 2020.

[24] Makinejad, K. et al. "A lumped electro-thermal model for Li-ion cells in electric vehicle application". *World Electric Vehicle Journal* **7**.1 (2015), 1–13.

[25] Alhanouti, M. et al. "New electro-thermal battery pack model of an electric vehicle". *Energies* **9**.7 (2016), 563.

[26] Gao, Z. et al. "Integrated equivalent circuit and thermal model for simulation of temperature-dependent LiFePO4 battery in actual embedded application". *Energies* **10**.1 (2017), 85.

[27] Gottapu, M. et al. "Fully coupled simplified electrochemical and thermal model for series-parallel configured battery pack". *Journal of Energy Storage* **36** (2021), 102424.

[28] Shabani, B. and Biju, M. "Theoretical modelling methods for thermal management of batteries". *Energies* **8**.9 (2015), 10153–10177.

[29] Astaneh, M. et al. "Calibration Optimization Methodology for Lithium-Ion Battery Pack Model for Electric Vehicles in Mining Applications". *Energies* **13**.14 (2020), 3532.

[30] Nagasubramanian, G. "Electrical characteristics of 18650 Li-ion cells at low temperatures". *Journal of applied electrochemistry* **31**.1 (2001), 99–104.

[31] Zhang, S., Xu, K., and Jow, T. "The low temperature performance of Li-ion batteries". *Journal of Power Sources* **115**.1 (2003), 137–140.

[32] Fan, J. and Tan, S. "Studies on charging lithium-ion cells at low temperatures". *Journal of The Electrochemical Society* **153**.6 (2006), A1081.

[33] Petzl, M., Kasper, M., and Danzer, M. A. "Lithium plating in a commercial lithium-ion battery–A low-temperature aging study". *Journal of power sources* **275** (2015), 799–807.

[34] Smart, M., Ratnakumar, B., and Surampudi, S. "Electrolytes for Low-Temperature Lithium Batteries Based on Ternary Mixtures of Aliphatic Carbonates". *Journal of the Electrochemical Society* **146**.2 (1999), 486.
[35] Plichta, E. and Behl, W. "A low-temperature electrolyte for lithium and lithium-ion batteries". *Journal of Power Sources* **88**.2 (2000), 192–196.
[36] Huang, C.-K. et al. "The limits of low-temperature performance of Li-ion cells". *Journal of the Electrochemical Society* **147**.8 (2000), 2893.
[37] Lin, H.-P. et al. "Low-temperature behavior of Li-ion cells". *Electrochemical and solid state letters* **4**.6 (2001), A71.
[38] Wang, C., Appleby, A. J., and Little, F. E. "Low-temperature characterization of lithium-ion carbon anodes via microperturbation measurement". *Journal of the Electrochemical Society* **149**.6 (2002), A754.
[39] Shidore, N. and Bohn, T. "Evaluation of cold temperature performance of the JCS-VL41M PHEV battery using Battery HIL". Tech. rep. SAE Technical Paper, 2008.
[40] Lustbader, J. A. et al. "Range Extension Opportunities While Heating a Battery Electric Vehicle" (2018).
[41] Lustbader, J. A. et al. "Total Thermal Management of Battery Electric Vehicles (BEVs)". Tech. rep. National Renewable Energy Lab.(NREL), Golden, CO (United States), 2018.
[42] Yuksel, T. and Michalek, J. J. "Effects of regional temperature on electric vehicle efficiency, range, and emissions in the United States". *Environmental science & technology* **49**.6 (2015), 3974–3980.
[43] Taggart, J. "Ambient temperature impacts on real-world electric vehicle efficiency & range". *2017 IEEE Transportation Electrification Conference and Expo (ITEC)*. IEEE. 2017, pp. 186–190.
[44] Meyer, N. et al. "The impact of driving cycle and climate on electrical consumption & range of fully electric passenger vehicles". *Proceedings of EVS*. Vol. 26. 2012, p. 11.
[45] Steinstraeter, M., Heinrich, T., and Lienkamp, M. "Effect of Low Temperature on Electric Vehicle Range". *World Electric Vehicle Journal* **12**.3 (2021), 115.
[46] Chen, D. et al. "Comparison of different cooling methods for lithium ion battery cells". *Applied Thermal Engineering* **94** (2016), 846–854.
[47] Jarrett, A. and Kim, I. Y. "Design optimization of electric vehicle battery cooling plates for thermal performance". *Journal of Power Sources* **196**.23 (2011), 10359–10368.
[48] Jarrett, A. and Kim, I. Y. "Influence of operating conditions on the optimum design of electric vehicle battery cooling plates". *Journal of Power sources* **245** (2014), 644–655.
[49] Zhu, L. et al. "Thermal analysis and optimization of an EV battery pack for real applications". *International Journal of Heat and Mass Transfer* **163** (2020), 120384.
[50] Pulugundla, G., Dubey, P., and Srouji, A. "Time-accurate CFD analysis of liquid cold plates for efficient thermal performance of electric vehicle Li-ion battery modules". Tech. rep. SAE Technical Paper, 2019.

[51] Shang, Z. et al. "Structural optimization of lithium-ion battery for improving thermal performance based on a liquid cooling system". *International Journal of Heat and Mass Transfer* **130** (2019), 33–41.
[52] Zhang, T. et al. "Investigation on the promotion of temperature uniformity for the designed battery pack with liquid flow in cooling process". *Applied Thermal Engineering* **116** (2017), 655–662.
[53] Ji, Y. and Wang, C. Y. "Heating strategies for Li-ion batteries operated from subzero temperatures". *Electrochimica Acta* **107** (2013), 664–674.
[54] Lei, Z., Zhang, Y., and Lei, X. "Improving temperature uniformity of a lithium-ion battery by intermittent heating method in cold climate". *International Journal of Heat and Mass Transfer* **121** (2018), 275–281.
[55] Qu, Z., Jiang, Z., and Wang, Q. "Experimental study on pulse self–heating of lithium–ion battery at low temperature". *International Journal of Heat and Mass Transfer* **135** (2019), 696–705.
[56] Zhang, C., Jin, X., and Li, J. "PTC self-heating experiments and thermal modeling of lithium-ion battery pack in electric vehicles". *Energies* **10**.4 (2017), 572.
[57] Hande, A. and Stuart, T. "AC heating for EV/HEV batteries". *Power Electronics in Transportation, 2002.* IEEE. 2002, pp. 119–124.
[58] Stuart, T. and Hande, A. "HEV battery heating using AC currents". *Journal of Power Sources* **129**.2 (2004), 368–378.
[59] Zhu, J. et al. "An alternating current heating method for lithium-ion batteries from subzero temperatures". *International Journal of Energy Research* **40**.13 (2016), 1869–1883.
[60] Hu, X. et al. "Battery warm-up methodologies at subzero temperatures for automotive applications: Recent advances and perspectives". *Progress in Energy and Combustion Science* **77** (2020), 100806.
[61] Ling, Z. et al. "Warming-up effects of phase change materials on lithium-ion batteries operated at low temperatures". *Energy Technology* **4**.9 (2016), 1071–1076.
[62] Ouyang, D. et al. "Influence of low temperature conditions on lithium-ion batteries and the application of an insulation material". *RSC advances* **9**.16 (2019), 9053–9066.
[63] Wu, H. et al. "Experimental study on aerogel passive thermal control method for cylindrical lithium-ion batteries at low temperature". *Applied Thermal Engineering* **169** (2020), 114946.
[64] Technologies, G. "GT-SUITE Flow Theory Manual". 2020.
[65] Kays, W. M. "Convective heat and mass transfer". Tata McGraw-Hill Education, 2011.
[66] Ghiaasiaan, S. M. "Convective heat and mass transfer". CRC Press, 2018.
[67] Huria, T. et al. "High fidelity electrical model with thermal dependence for characterization and simulation of high power lithium battery cells". *2012 IEEE International Electric Vehicle Conference*. IEEE. 2012, pp. 1–8.
[68] Sun, Q. et al. "Adaptive unscented kalman filter with correntropy loss for robust state of charge estimation of lithium-ion battery". *Energies* **11**.11 (2018), 3123.
[69] Singer, S. and Nelder, J. "Nelder-mead algorithm". *Scholarpedia* **4**.7 (2009), 2928.

[70] Pesaran, A., Santhanagopalan, S., and Kim, G. "Addressing the impact of temperature extremes on large format li-ion batteries for vehicle applications (presentation)". Tech. rep. National Renewable Energy Lab.(NREL), Golden, CO (United States), 2013.

[71] Tete, P. R., Gupta, M. M., and Joshi, S. S. "Developments in battery thermal management systems for electric vehicles: A technical review". *Journal of Energy Storage* **35** (2021), 102255.

[72] Barlow, T. J. et al. "A reference book of driving cycles for use in the measurement of road vehicle emissions". *TRL Published Project Report* (2009).